Positive magnetoresistance in anapole superconductor junctions

Tim Kokkeler,[1,2,*] Alexander Golubov,[2] and Yukio Tanaka[3,4]
[1]*Donostia International Physics Center (DIPC), 20018 Donostia–San Sebastián, Spain*
[2]*ICE (TNW), University of Twente, 7522 NB Enschede, Netherlands*
[3]*Deparment of Applied Physics, Nagoya University, 464-8603 Nagoya, Japan*
[4]*Research Center for Crystalline Materials Engineering, Nagoya University, 464-8603 Nagoya, Japan*

(Received 4 December 2023; revised 15 February 2024; accepted 10 April 2024; published 8 May 2024)

This paper presents a method to detect time-reversal symmetry breaking in noncentrosymmetric superconductors using only transport measurements. Specifically, if time-reversal symmetry is broken via a phase difference between singlet and triplet correlations, as in anapole superconductors, the differential conductance in superconductor-ferromagnet-normal metal junctions is enhanced by increasing the exchange field strength in the ferromagnet. This is in sharp contrast with the negative magnetoresistance when using superconductors in which time-reversal symmetry is preserved. Moreover, results show a large quadrupolar component of the magnetoresistance which is qualitatively different from the bipolar giant magnetoresistance in strong ferromagnets.

DOI: 10.1103/PhysRevB.109.174513

I. INTRODUCTION

Recent advances within superconductivity focus on the understanding of unconventional superconductors [1–5], i.e., superconductors which do not obey BCS theory. In unconventional superconductors, triplet [1,6–25] and odd-frequency [8,26–37] pairings may appear. Most attention is paid to superconductors in which inversion ($\mathcal{P}$) and time-reversal ($\mathcal{T}$) symmetry are preserved in the pair potential. However, several known superconductors break time-reversal symmetry, either in bulk or near the edges [1,7,15,38–74], while for superconductors in which the crystal structure breaks inversion symmetry, the pair potential may contain both even- and odd-parity components [13,75–86]. Also, the breaking of translation symmetry near an edge may cause a local admixture of even-parity and odd-parity superconductivity [87,88].

Moreover, in a recently discussed class of superconductors, anapole superconductors, both symmetries are broken [89–94]. Examples of possible anapole superconductors are UTe_2 [89–91], $Cu_xBi_2Se_3$, and $Sn_{1-x}In_xTe$ [92], while also noncentrosymmetric superconductors with a magnetic ordering in their phase diagram, such as $CePt_3Si$ [13], UIr [76], $CeRh_2As_2$ [95], and $CeCu_2Si_2$ [96], are promising platforms for $\mathcal{P}$ and $\mathcal{T}$ broken superconducting phases in some parameter regimes. Next to this, time-reversal symmetry can be broken via the inverse proximity effect of a ferromagnet or ferromagnetic insulator [97]. Thus, both noncentrosymmetric and time-reversal symmetry broken superconductivity is abundant. The proximity effect of superconductors that are time-reversal and/or inversion symmetry broken can be significantly different from the proximity effect of superconductors in which these symmetries are preserved [85,98–106].

Superconductors in which both time-reversal symmetry and inversion symmetry are broken have great potential for future applications, for example, in nonreciprocal transport, since the conditions for nonreciprocal transport to occur, time-reversal symmetry breaking and gyrotropy [107,108], are met intrinsically in the bulk material. Therefore, such superconductors are a promising platform for superconducting diodes [45,87,109–149], no external source of an exchange field and/or spin-orbit coupling is needed. This greatly simplifies the setup for such diodes.

The proximity effect and transport properties of noncentrosymmetric or time-reversal symmetry broken superconductors have been studied in detail in several limits [85,98–104,150–157]. Recently, a dirty limit transport theory was discussed, focusing on $(i)s+p$-wave superconductors [87,106]. In such superconductors, the pair potential breaks inversion symmetry as indicated by the simultaneous presence of even-parity s-wave and odd-parity p-wave components, while time-reversal symmetry is broken if the phase difference between the singlet and triplet correlations is not a multiple of π. In Ref. [106], the importance of considering time-reversal symmetry breaking of the pair potential of superconductors was illustrated using superconductor-normal metal-normal metal (SNN) junctions. However, in SNN junctions the dependence of the differential conductance on the phase between the singlet and triplet components cannot be unambiguously distinguished from the dependence on the ratio of their magnitudes. Therefore, a method to obtain smoking-gun evidence for time-reversal symmetry breaking based only on transport measurements is so far absent.

In this paper, we provide such method by showing that time-reversal symmetry breaking in the superconductor can be identified using superconductor-ferromagnet-normal metal (SFN) junctions. We show that for the time-reversal symmetry broken noncentrosymmetric $is+p$-wave superconductors, the differential conductance for voltages just

*tim.kokkeler@dipc.org

below the superconducting gap can be strongly enhanced by an exchange field. This is in contrast with the negative magnetoresistance in noncentrosymmetric superconductors that obey time-reversal symmetry such as $s + p$-wave superconductors [158].

Moreover, the dependence of the differential conductance enhancement on the exchange field direction provides an additional tool to determine the direction of the d vector of the p-wave correlations. We show that if the exchange field strength h is much smaller than the Fermi energy E_F ($h/E_F \ll 1$), the magnetoresistance is quadrupolar, and the differential conductance is maximized when d-vector and exchange field are perpendicular. Thus, for ferromagnets with $h/E_F \ll 1$ the anisotropy of the magnetoresistance is qualitatively different from the well-known bipolar effects for $h/E_F \sim 1$ [159–166].

Next to this, we show that the voltage window in which the differential conductance is enhanced is determined by the ratio of the s-wave and p-wave components of the superconductors. In this way, time reversal symmetry breaking can be established and all parameters needed to fully describe the pair potential of single band $(i)s + p$-wave superconductors can be determined even in the absence of time reversal symmetry. The proposed method involves only transport measurements and therefore uses only well-known techniques. The results can be compared with other techniques that are used to detect time-reversal symmetry breaking, inversion symmetry breaking, or triplet pairing, such as the detection of diode effects in Josephson junctions [45,87,109–149], muon spin relaxation [167,168], critical magnetic field measurements [169,170], or nuclear magnetic resonance studies [16,44,171–174].

The setup of the paper is as follows. In Sec. II, we present the model for an SFN junction with time-reversal and inversion symmetry broken superconductors. In Sec. III, we show the differential conductance calculated using this model for $(i)s +$ helical p-wave superconductors. Next, in Sec. IV we present the results for $(i)s +$ chiral p-wave superconductors and compare them to those of $(i)s +$ helical p-wave superconductors. We conclude our article in Sec. V with a discussion of our results and discuss how to generalize to other types of noncentrosymmetric time-reversal broken superconductors.

II. MODEL

We study a junction in which a bar (F) with an exchange field is sandwiched between an unconventional superconductor and a normal metal electrode, schematically shown in Fig. 1. The model used is similar to the one used in Ref. [106], with the difference that an exchange interaction is included in the bar. We assume that the superconductivity and ferromagnetism are weak enough that we may use the quasiclassical formalism, $h/E_F, \Delta/E_F \ll 1$. This assumption is valid in weak ferromagnets or normal metals proximized by a ferromagnetic insulator. The induced exchange field causes Larmor precession of the electrons. Without the proximity effect, this does not affect the equilibrium properties of the metal, it only affects the distribution functions. However, if pair correlations exist, the presence of Larmor precession implies that while the spins of the pairs are still antiparallel when measured at the same time, they are, in general, not parallel when measured at different times. Thus, there is singlet-triplet conversion where

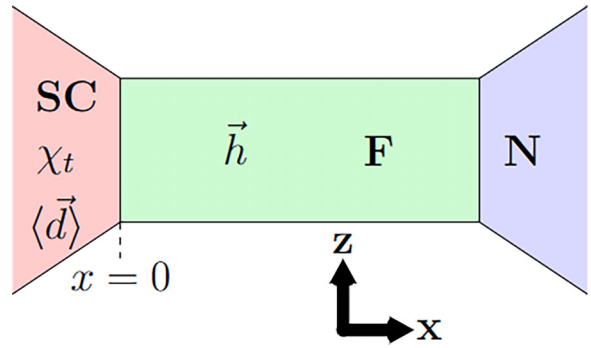

FIG. 1. A schematic of the SFN junction. The superconductor (SC) is characterized by the phase difference χ_t between the singlet and triplet components and by the d vector of the triplet component. The ferromagnet (F) is characterized by its exchange field. Both the SC and the normal metal (N) serve as electrodes.

the d vector of the triplets is parallel to the exchange field direction [175]. In S/F bilayers, this leads to spin splitting of the superconductor [175].

We assume that the scattering length in the problem is much smaller than any other relevant length scale, except the Fermi length, as is likely in thin films [176,177]. In this case, the Green's function is almost isotropic, and the Keldysh Usadel formalism [178,179] may be used to describe the F bar. We use the basis $(\psi_\uparrow, \psi_\downarrow, \psi_\downarrow^\dagger, -\psi_\uparrow^\dagger)^T$, so singlet components of the pair potential are proportional to the identity matrix in spin space, whereas the triplet components come along with spin-Pauli matrices. If the width of the bar is either much larger or much smaller than the thermal coherence length, an effective one-dimensional model may be used. In this limit, the Green's function $\bar{G}$ is approximately independent of the y and z coordinates,

$$D\partial_x(\bar{G}\partial_x\bar{G}) = [i(E + \boldsymbol{h}\cdot\boldsymbol{\sigma})\tau_3, \bar{G}], \tag{1}$$

where D is the spatially invariant diffusion constant, $\boldsymbol{\sigma}$ is the vector of Pauli matrices in spin space, $\bar{G}$ is the isotropic component of the Green's function, E is energy, and $\boldsymbol{h}$ is the exchange field in the ferromagnet, with magnitude h. If the interface resistance of the F/N interface is very small, for example, if the F bar is a normal metal proximized by a ferromagnetic insulator (FI) and the N electrode is the same normal metal, the Green's function is continuous at the F/N interface,

$$\bar{G}(x = L) = \bar{G}_N, \tag{2}$$

where $\bar{G}_N = \left[\begin{smallmatrix} \check{G}_N^R & \check{G}_N^K \\ 0 & \check{G}_N^A \end{smallmatrix}\right]$ is the Green's function in the normal metal electrode, where the retarded Green's function is $\check{G}_N^R = \tau_3$, the advanced Green's function is $\check{G}_N^A = -\tau_3$. The Keldysh Green's function is given by $\check{G}_N^K = \check{G}_N^R\check{h}_N - \check{h}_N\check{G}_N^A$, where $\check{h}_N = \hat{f}_{L0}\otimes\tau_0 + \hat{f}_{T0}\otimes\tau_3$ is the matrix distribution function, with the longitudinal (L) and transverse (T) components [180,181] determined by the Fermi-Dirac distribution: $\hat{f}_{L0,T0} = \frac{1}{2}(\tanh\frac{E+eV}{2k_BT} \pm \tanh\frac{E-eV}{2k_BT})$, where V is the voltage applied to the normal metal electrode, T is the temperature of the system, which we assume to be well below T_c, so we may use $T = 0$ in our calculations, and k_B is the Boltzmann constant.

We assume that both the S and the N junctions are electrodes, while the F layer is a restriction between these two. In that case, the inverse proximity effect of the ferromagnet on the clean $(i)s + p$-wave superconductor may be ignored, and the Tanaka-Nazarov boundary conditions [87,182,183], the extension of Nazarov's boundary conditions [184] to interfaces with unconventional superconductors, may be used. The boundary condition at the S/F interface reads

$$\bar{G}\nabla\bar{G}(x=0) = \frac{1}{\gamma_{BS}L}\langle\bar{S}(\phi)\rangle\,, \tag{3}$$

$$\bar{S}(\phi) = \tilde{T}\left(1 + T_1^2 + T_1(\bar{C}\bar{G} + \bar{G}\bar{C})\right)^{-1}(\bar{C}\bar{G} - \bar{G}\bar{C})\,, \tag{4}$$

$$\bar{C} = \bar{H}_+^{-1}(\bar{\mathbf{1}} - \bar{H}_-)\,, \tag{5}$$

$$\bar{H}_+ = \tfrac{1}{2}(\bar{G}_S(\phi) + \bar{G}_S(\pi - \phi))\,, \tag{6}$$

$$\bar{H}_- = \tfrac{1}{2}(\bar{G}_S(\phi) - \bar{G}_S(\pi - \phi))\,, \tag{7}$$

where ϕ is the angle of the mode with the normal to the interface. We assume that the bar is wide enough that many modes can pass through the interface, that is, the problem is not fully one-dimensional. Averaging over all modes passing through the interface is denoted by $\langle\cdot\rangle$, and $\gamma_{BS} = R_B/R_d$ is the ratio between the boundary resistance and the normal state resistance, that is, the resistance in the absence of the superconducting proximity effect of F, and the parameter $T_1 = \tilde{T}/(2 - \tilde{T} + 2\sqrt{1-\tilde{T}})$ [183], where $\tilde{T}$ is the interface transparency given by

$$\tilde{T}(\phi) = \frac{\cos^2\phi}{\cos^2\phi + z^2}\,, \tag{8}$$

with z the Blonder-Tinkham-Klapwijk (BTK) parameter. The retarded part of the Green's function of the superconductor $\bar{G}_S(\phi)$ is given by the bulk equilibrium Green's function of an $(i)s + p$-wave superconductor. For $is + p$-wave superconductors, the pair potential is given by

$$\Delta(\phi)/\Delta_0 = e^{i\frac{\pi}{2}\chi_t}\frac{1}{\sqrt{r^2+1}} + \frac{r}{\sqrt{r^2+1}}\boldsymbol{d}(\phi)\cdot\boldsymbol{\sigma}, \tag{9}$$

where $\boldsymbol{d}(\phi)$ is the d vector, an angle dependent unit vector that is different for different types of p-wave superconductors, χ_t is the phase difference between the singlet and triplet components, Δ_0 is the energy scale of the pair potentia, and r is the mixing parameter. Therefore, the bulk Green's function reads [185]

$$\begin{aligned}\check{G}_S^R(\phi) = {}& \frac{1}{2}(1 + \hat{\boldsymbol{d}}(\phi)\cdot\boldsymbol{\sigma}) \otimes \frac{1}{\sqrt{E^2 - |\Delta_+|^2}}\begin{bmatrix} E & \Delta_+ \\ -\Delta_+^* & -E\end{bmatrix} \\ & + \frac{1}{2}(1 - \hat{\boldsymbol{d}}(\phi)\cdot\boldsymbol{\sigma}) \\ & \otimes \frac{1}{\sqrt{E^2 - |\Delta_-|^2}}\begin{bmatrix} E & \Delta_- \\ -\Delta_-^* & -E\end{bmatrix}, \\ \Delta_\pm = {}& \frac{e^{i\frac{\pi}{2}\chi_t} \pm re^{i\psi(\phi)}}{\sqrt{r^2+1}}\,,\end{aligned} \tag{10}$$

where $\psi(\phi)$ is the phase of the d vector, which may depend on the mode, and $\hat{\boldsymbol{d}}(\phi) = \boldsymbol{d}(\phi)/e^{i\psi(\phi)}$. while its distribution function is the equilibrium Fermi-Dirac distribution. The advanced and Keldysh components can now be found using, respectively, $\check{G}_S^A = -\tau_3(\check{G}_S^R)^\dagger\tau_3$ and $\check{G}_S^K = \check{G}_S^R\check{h}_S - \check{h}_S\check{G}_S^A$, with $\check{h}_S = \tanh E/(2k_BT)\mathbf{1}$. The following set of parameters is used throughout the paper: $\gamma_{BS} = 2$, $z = 0.75$, $E_{\rm Th}/\Delta_0 = 0.02$, where $E_{\rm Th} = D/L^2$ is the Thouless energy of the junction, with D specifying the diffusion constant and L the length of the junction, to compare with the results on noncentrosymmetric superconductors in previous articles [106,158].

III. HELICAL *P*-WAVE SUPERCONDUCTORS

First, we focus on $(i)s +$ helical p-wave superconductors, that is, the helical p-wave component has d vector,

$$\boldsymbol{d}(\phi) = (\cos\phi, \sin\phi, 0), \tag{11}$$

which implies that $\hat{\boldsymbol{d}}(\phi) = \boldsymbol{d}(\phi)$ and $\psi(\phi) = 0$ for helical superconductors. We contrast the results for $is +$ helical p-wave ($\chi_t = 1$) superconductors with those obtained for $s +$ helical p-wave ($\chi_t = 0$) superconductors in Ref. [158], and then provide an explanation for their differences.

The exchange field dependence of the differential conductance of an SFN junction with $is +$ helical p-wave superconductors is shown in Fig. 2 for s-wave dominant superconductors ($r = 0.5$) and Fig. 3 for helical p-wave dominant superconductors ($r = 2$). In both Figs. 2 and 3, the left panel corresponds to a parallel orientation of $\boldsymbol{h}$ and $\langle\boldsymbol{d}\rangle$, while the right panel corresponds to the perpendicular orientation of these two vectors. In all panels, there is a zero-bias conductance peak with a width of the order of the Thouless energy for $h = 0$. This peak is due to coherent Andreev reflection and is split into two peaks at $|eV| = h$ for all orientations of the field, even if the helical p-wave component is dominant, in contrast to the $s +$ helical p-wave superconductors. For $s +$ helical p-wave pairing, the topological ZESABS felt by the perpendicular injected quasiparticles does not change as far as $\Delta_p > \Delta_s$ [158,186]. On the other hand, for the $is +$ helical p-wave superconductor, even if the magnitude of the s-wave component is infinitesimal, the topological protection is broken and the ZBCP splits. This is due to the presence of both singlet and triplet components at $E = 0$ in the presence of time-reversal symmetry breaking [106]. In the helical p-wave dominant case, a small zero bias peak remains if $\boldsymbol{h}$ and $\langle\boldsymbol{d}\rangle$ are perpendicular due to the long-range triplets [187], see Fig. 3(b), and in all other cases the zero bias conductance peak is converted into a zero bias conductance dip, see Figs. 2 and 3(a). The height of the peak decreases for increasing exchange field strength, for $h \gg \Delta_0$ it is diminished.

If the s-wave component is dominant, $r < 1$, shown in Fig. 2, there is a sharp peak in the differential conductance around $|eV| = \Delta_0$. This peak, which is due to a suppression of the boundary resistance, is enhanced in the presence of an exchange field. If the field is parallel to the d vector of the helical p-wave component, this enhancement is only to a small extent apparent for large fields, i.e., $h \gg \Delta_0$ and for $eV \approx \Delta_0$, for which the bound states are due to oblique modes, as shown in Fig. 2(a). On the other hand, if $\boldsymbol{h}$ is perpendicular to $\langle\boldsymbol{d}\rangle$, a small field is enough to increase the differential conductance of the junction, as shown in Fig. 2(b). In both cases, the differential conductance does not increase indefinitely, but saturates at a value that is slightly higher for the perpendicular

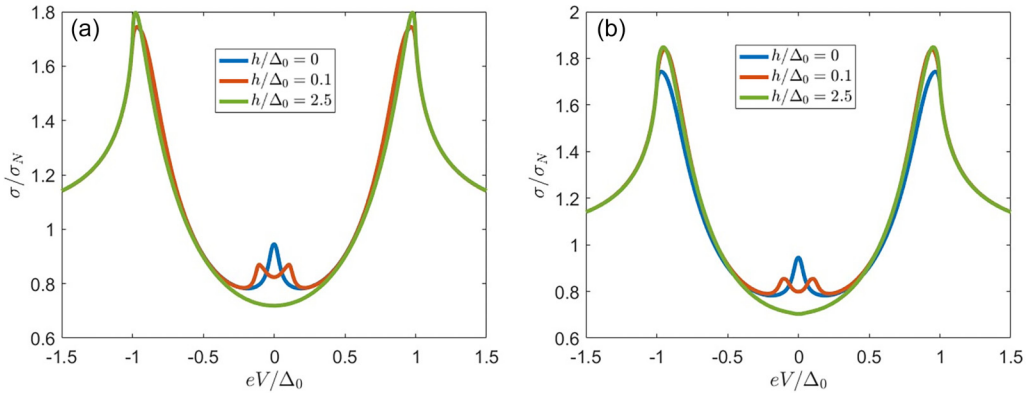

FIG. 2. The magnetic field dependence of the differential conductance of *is* + helical *p*-wave junctions for $\chi_t = 1$ for parallel (a) and perpendicular (b) orientations when $r = 0.5$. The sharp peak that without magnetic field is at zero bias splits into two peaks at $|eV| = h$ for small h, disappearing completely for large h. For voltages just below Δ_0, the differential conductance is enhanced by the exchange field. This effect is stronger for the perpendicular orientation than for the parallel orientation.

orientation than for the parallel orientation. The maximum increase of conductance is of the order of $0.1\sigma_N$.

If the helical *p*-wave component is dominant, $r > 1$, the peak just below $|eV| = \Delta_0$ is much wider, as shown in Fig. 3. Also in this case, the differential conductance is enhanced by an exchange field. In the parallel orientation, this enhancement only appears in a small window around $|eV| = 0.8\Delta_0$, is relatively small, and can be found only for large fields, see Fig. 3(a). This difference is difficult to measure in experiment. For the perpendicular orientation, on the other hand, the enhancement appears in a large window and is largely enhanced compared to parallel field for small fields $h \ll \Delta_0$. If the field is parallel, a conductance enhancement of a few percent can be achieved; for the perpendicular orientation, an enhancement of $0.1\sigma_N$ can be achieved, as in the case $r < 1$. Comparing this to the magnetoresistance in s + helical *p*-wave superconductors [158], we find that the magnetoresistance in *is* + helical *p*-wave superconductors has opposite signs and a much stronger anisotropy. The difference between these materials is due to the presence or absence of time-reversal symmetry. For s + helical *p*-wave superconductors, time-reversal symmetry is not broken. Moreover, in a dirty material, the scattering rate is high and therefore the Green's function is almost isotropic. Therefore, the density of states in the surface Green's function $\bar{C}$ is independent of spin. On the other hand, for the *is* + helical *p*-wave superconductor, time-reversal symmetry is broken, and the surface density of states is different for spins parallel or antiparallel to $\langle \boldsymbol{d} \rangle$.

Based on this knowledge, the differential conductance enhancement can be inferred from the Tanaka-Nazarov boundary conditions, specifically, the Keldysh component [23]. If the density of states of the surface Green's function has no spin dependence, as for the s + helical *p*-wave superconductor, the only difference in the commutator or anticommutator in the expressions of this boundary condition caused by the exchange field comes from the terms of diagonal in Nambu space. Since the pair amplitude in the normal metal is suppressed by a finite boundary resistance, the off-diagonal terms are small and hence the effect of the exchange field on the anticommutator is small in this case.

On the other hand, for the *is* + helical *p*-wave case, the density of states of the surface Green's function also has a

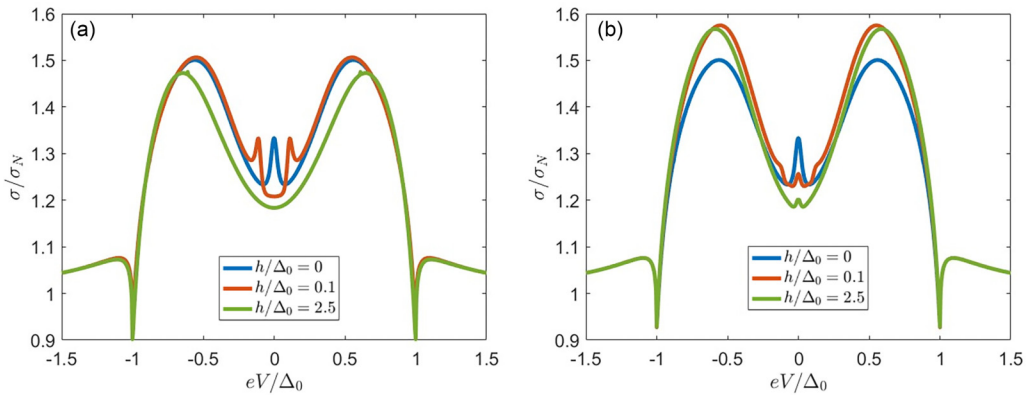

FIG. 3. The magnetic-field dependence of the differential conductance of *is* + helical *p*-wave junctions for $\chi_t = 1$ and $r = 2$ for parallel (a) and perpendicular (b) orientations of the exchange field with respect to the d vector. The sharp peak that without magnetic field is at zero bias splits into two peaks at $|eV| = h$ for small h, disappearing for large h. For voltages just below Δ_0, the differential conductance is enhanced by the exchange field. This effect is stronger for the perpendicular orientation than for the parallel orientation.

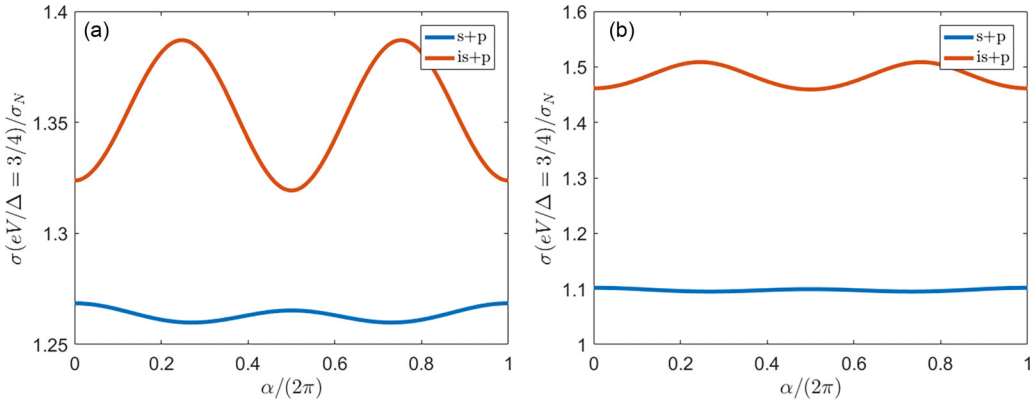

FIG. 4. The quadrupolar dependence of the differential conductance of $is+$ helical p-wave junctions at $eV/\Delta_0 \approx 0.75$ on the angle α between the exchange field and d vector of the superconductor for $r = 0.5$ (a) and $r = 2$ (b). The exchange field strength is $h/\Delta_0 = 0.2$. For $s+$ helical p-wave superconductors, the differential conductance is maximized for the parallel orientation. On the other hand, for $is+$ helical p-wave superconductors, the differential conductance is minimized in the parallel orientation and the angular dependence is much larger. There is also a small bipolar component, $\sigma(\alpha = \pi) \neq \sigma(\alpha = 0)$, however, the quadrupolar component dominates.

spin dependence and hence the contribution of the density states to the anticommutator in the Tanaka-Nazarov boundary condition depends on the exchange field. This reduces the eigenvalues of the anti commutator $\bar{C}\bar{G} + \bar{G}\bar{C}$. This implies that the enhancement of the differential conductance is largest for those voltages for which $T_1(\bar{C}\bar{G} + \bar{G}\bar{C})$ is the dominant term in the denominator. As shown in Ref. [106], for $is+$ helical p-wave superconductors, this term is dominant for $\frac{1}{\sqrt{r^2+1}} < |eV|/\Delta_0 < 1$. Thus, the enhancement of the differential conductance is most prominent in a broader voltage window if the helical p-wave component of the pair potential is larger.

To understand the physical mechanism behind the enhancement of conductance just below $|eV| = \Delta_0$, we first consider the physical interpretation of the denominator. We consider a junction between two materials, called material 1 and material 2. Both materials have a spin-dependent density of states, and at most one of them is a superconductor. An example of such system is the S/F junction with proximity effect studied in this paper. From the derivation in Ref. [184], it follows that the denominator can be attributed to higher order tunneling. Indeed, to first order in the tunneling T_1 parameter between two materials with Green's functions $\bar{G}_{1,2}$, the current between these materials is given by $T_1[\bar{G}_1, \bar{G}_2]$, the well-known Kuprianov-Luckichev boundary condition [188]. Thus, in the Tanaka-Nazarov boundary condition [182], it is only upon inclusion of the higher orders in T_1 that the denominator makes a difference, and it suppresses the first-order approximation. The Green's function exactly at the interface between the superconducting electrode and the bar is altered by the tunneling of the electrons of the other material into it. Therefore, the difference in Green's functions on either side of the interface is smaller, leading to a reduction of the current compared to the first order estimation.

Next we consider the effect of the relative orientation of the spin quantization axes in the two materials on these higher order terms. Suppose a fraction ϵ of electrons is exchanged between materials 1 and 2 due to the tunneling. If the spin quantization axis is the same for both materials 1 and 2,

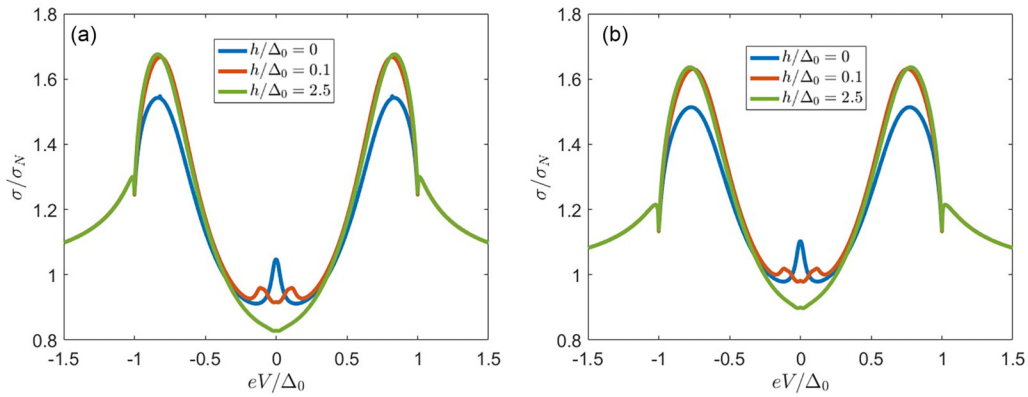

FIG. 5. The magnetic-field dependence of the differential conductance of $is+$ helical p-wave junctions for $\chi_t = 1$ for $r = 0.9$ (a) and $r = 1.1$ (b) when the field is perpendicular to the d vector. The sharp peak that without magnetic field is at zero bias splits into two peaks at $|eV| = h$ for small h, disappearing completely for large h. The increase in the differential conductance by applying a magnetic field is larger than for $r = 0.5$ or $r = 2$, confirming that it is an effect for which the coexistence of even and odd-parity contributions to the pair potential.

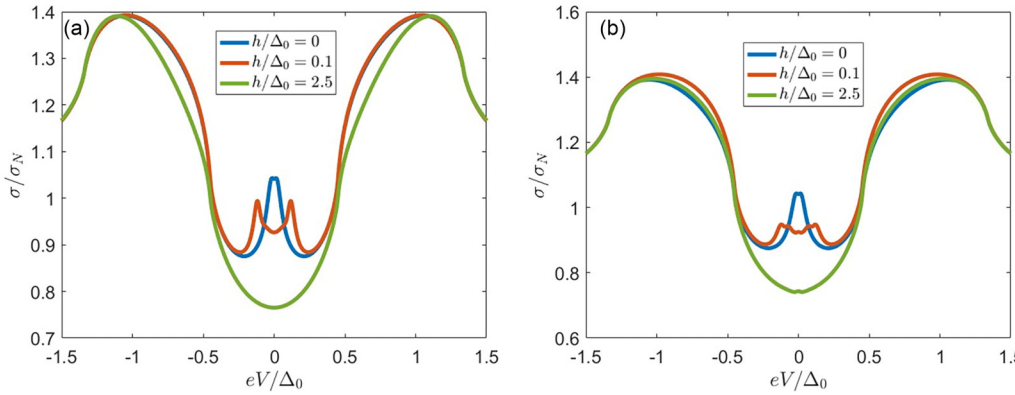

FIG. 6. The differential conductance in $is+$ chiral p-wave junctions in the presence of parallel (a) and perpendicular (b) exchange fields. The presence of a small exchange field can increase the differential conductance in the junction. The increase is less visible then for $is+$ helical p-wave junctions because the phase is mode dependent. Therefore, only the differential conductance of a selection of modes is enhanced, while that of the others is suppressed. The superconductor is s-wave dominant, with $r = 0.5$.

the resulting new pair amplitudes and density of states are a weighted average of the two Green's functions.

This is not the case if the spin quantization axes in the superconductor and ferromagnet are perpendicular, for example along the z axis in material 1 and along the x axis in material 2. The electrons moving from 2 to 1 do contribute to all spin-averaged properties, i.e., to those parts of the Green's function proportional to σ_0. However, the electrons that move from 2 to 1 do not have any spin projection along the z axis. Thus, the change in the σ_z term of the Green's function in 1 is much smaller in the perpendicular orientations. Likewise, the electrons moving from material 1 do not have any spin projection along the x direction and therefore the σ_x term of the Green's function is much less altered than in the parallel case.

One may use an analogy with vectors in real space. If one adds two parallel or antiparallel vectors, the length of this vector changes significantly. On the other hand, if one adds a small vector perpendicular to the first vector, there is only a small rotation, no change in the projection along the axis of the initial vector, and, moreover, to first order, no length change of the vector. We note that this analogy should not be considered literally. In the junction, the formalism is a bit more difficult because we consider matrices in Keldysh-Nambu-spin space, but the mechanism is qualitatively the same.

Thus, if the spin quantization axis is different in the two materials, the Green's functions at the interface remain more different compared to the case in which they are parallel. For this reason, the current is minimized if the d vector and ferromagnet are parallel. That the conductance in this orientation is lower than the normal state conductance can be understood using the anticommutator as well. Indeed, in the presence of a bound state, the elements of C diverge and hence $\{C, \tau_3\} \gg 2 = \{C, C\}$. Thus, a suppression of the pair amplitudes at the boundary by an exchange field leads to an enhancement of the anticommutator, and hence a suppression of conductance. This mechanism is suppressed in the perpendicular orientation of exchange field and angular averaged d vector since in this case the triplets are long-range.

In the setup used in this paper, the spin quantization axis of the surface Green's function is along the angular averaged d vector [158]. If the exchange field is not parallel

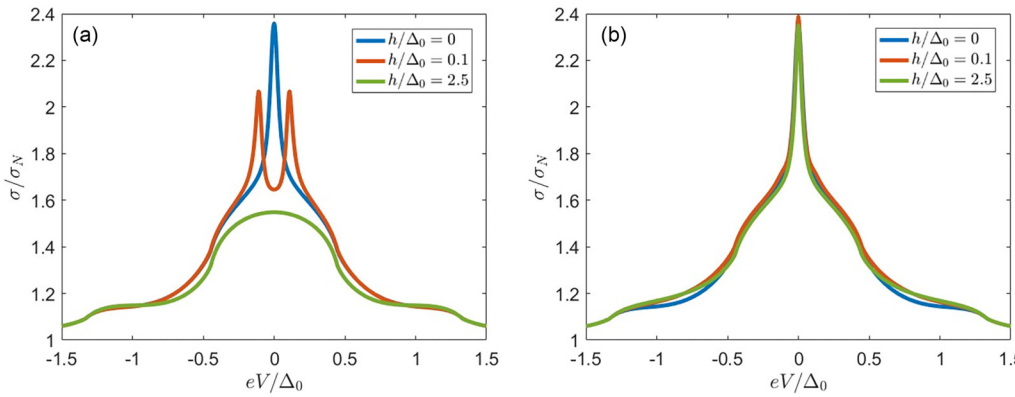

FIG. 7. The differential conductance in $is+$ chiral p-wave junctions in the presence of parallel (a) and perpendicular (b) exchange fields. The superconductor is p-wave dominant, with $r = 2$. The sharp zero-bias conductance peak splits upon application of a parallel exchange field, but hardly changes by application of a perpendicular field. This happens because the ZBCP is due to the oblique modes, for which the phase difference between the modes is almost 0.

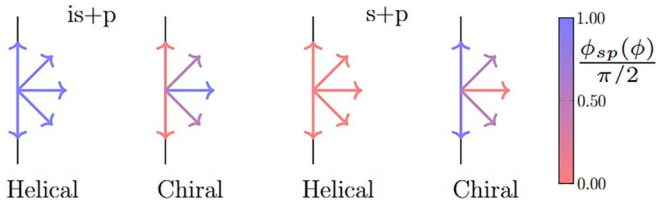

FIG. 8. Schematic showing the difference between helical and chiral $(i)s$ + p-wave superconductors. The phase difference between singlet and triplet superconductors $\phi_{sp}(\phi)$ is illustrated by color. For $(i)s$ + helical p-wave superconductors, this phase difference is independent of the direction of momentum, and hence all modes contribute to an enhancement of the differential conductance. On the other hand, for the $(i)s$ + chiral p-wave superconductor, the phase difference between the triplet and singlet components depends on the angle of momentum, and hence for some modes the differential conductance is enhanced while for others it is suppressed.

to the angular-averaged d vector, it rotates the quantization axes of the induced pair correlations in the ferromagnet. Meanwhile, since the exchange field is only present in the normal metal, the quantization axis of the superconductor is unchanged. Therefore, the current increases if the exchange field is not parallel to the d vector of the superconductor, explaining the enhancement of the differential conductance compared to the normal state and the anisotropy in the enhancement. This leads to a quadrupolar dependence of the differential conductance on the angle α between d vector and exchange field, as shown in Fig. 4. An enhancement of supercurrents [189] and a quadrupolar dependence of conductance on the exchange field in proximity structures has been found before [187]. The predicted effect, however, differs from Ref. [187] via the voltage range in which the effect appears.

Though smaller than for the perpendicular orientation, for the s-wave dominant case there is also an enhancement of conductance just below $|eV| = \Delta_0$ in the parallel orientation compared to the case with $h = 0$ as shown in Fig. 2(a). Also in the helical p-wave dominant case, there is a very small enhancement in this voltage window, see Fig. 3(a). This is a specific feature of the helical p-wave superconductor. Indeed, for the helical p-wave superconductor, the direction of the d vector is parallel to momentum, and therefore even if $\boldsymbol{h}$ and $\langle \boldsymbol{d} \rangle$ are parallel there exist modes for which $\boldsymbol{h}$ and $\boldsymbol{d}(\phi)$ are not, and hence the differential conductance is enhanced. Since the mode at normal incidence has the largest transmission eigenvalue, the enhancement in conductance if $\boldsymbol{h} \parallel \langle \boldsymbol{d} \rangle$ is small compared to the enhancement for $\boldsymbol{h} \perp \langle \boldsymbol{d} \rangle$.

The predicted sign and anisotropy of the magnetoresistance can only be found if the exchange field strength h is much smaller than the Fermi energy E_F. If the ferromagnetic interaction is significant compared to the Fermi energy, the difference in momenta for opposite spins is large. In that case, the differential conductance is maximized for the parallel orientation and minimized for the antiparallel orientation in F/S/F or F/F junctions [160,161]. In the quasiclassical formalism, such effects are suppressed by a factor h/E_F and therefore negligible compared to the effect described here as long as $h/E_F \ll 1$. The difference in symmetries between the two effects, in fact, allows one to disentangle them. Also, within the quasiclassical formalism there is a small bipolar component, however, this component is small compared to the quadrupolar component.

Because time-reversal symmetry is broken in the superconductor, for is + helical p-wave superconductors $r = 1$ is not a topological phase transition, unlike for the s + helical p-wave superconductor [2,190–192]. Therefore, the differential conductance is continuous as a function of r, both in the absence and presence of an exchange field, as confirmed by the results in Fig. 5. The obtained results do not depend qualitatively on the exact geometry, as illuminated in the Appendix. To obtain the largest enhancement and clearest difference between the two orientations, we recommend using a long junction characterized by a large BTK parameter z and a small ratio of boundary resistance to bar resistance γ_B.

IV. CHIRAL *P*-WAVE SUPERCONDUCTORS

The same calculations were performed for is + chiral p-wave superconductors, for which the d vector is given by

$$\boldsymbol{d}(\phi) = e^{i\phi}(0, 0, 1). \tag{12}$$

That is, $\hat{\boldsymbol{d}} = (0, 0, 1)$ and $\psi(\phi) = \phi$ for is + chiral p-wave superconductors. To compare results, we used the same set of parameters as for the junction with $(i)s$ + helical p-wave superconductors, that is, $\gamma_{BS} = 2$, $z = 0.75$, $E_{\mathrm{Th}}/\Delta_0 = 0.02$. The dependence of the differential conductance on the exchange field is illustrated in Fig. 6 for s-wave dominant superconductors and Fig. 7 for p-wave dominant superconductors. We first elaborate on the results and how they depend on parameters, then we provide a physical explanation for the differences compared to the $(i)s$ + helical p-wave junctions.

For is + chiral p-wave superconductors, a weak exchange field leads to an increase in the differential conductance for $eV \approx 0.8\Delta_0$ for all $r < 1$; see Fig. 6. Similar to the helical case, the enhancement for is + chiral p-wave superconductors is much stronger if the exchange field is perpendicular to the d vector [Fig. 6(b)] then if it is parallel to it [Fig. 6(a)]. The enhancement however, is smaller than for the s + helical p-wave superconductors, maximally around $0.05\sigma_N$ for the perpendicular orientation and almost negligible in the parallel orientation, and is smaller for larger exchange fields, as shown in 6(b).

For p-wave dominant is + chiral p-wave superconductors, there is a weak suppression of the zero bias conductance in the presence of an exchange field even for perpendicular fields [Fig. 7(b)], but it is very small compared to the parallel orientation; see Fig. 7(a). Correspondingly, the peaks at $|eV| = h$ only appear for parallel exchange fields. For $|eV| \approx 0.8\Delta_0$, the presence of an exchange field always decreases the differential conductance in junctions with s + chiral p-wave superconductors, as discussed in Ref. [158], whereas it increases the differential conductance for is + chiral p-wave superconductors, though the effect is considerably smaller than for helical p-wave superconductors. Thus, while the proposed method to determine the pair potential works well for s + helical p-wave superconductors, it does not do so if chiral p-wave superconductors are present. The difference between the $(i)s$ + chiral and $(i)s$ + helical p-wave superconductors

TABLE I. Summary of signatures of the differential conductance in SNN/SFN junctions using $(i)s+$ helical p-wave superconductors as found in Ref. [158] and this paper, based on the ratio of the zero bias conductance $\sigma(eV=0)$ at zero field and normal state resistance σ_N and the exchange field anisotropy in the voltage window $0 < eV_{\mathrm{ani,min}} < eV < eV_{\mathrm{ani,max}}$ and whether there exists an angle such that $\sigma(h\neq 0) > \sigma(h=0)$ within this voltage window. Each of the six categories has a unique combination of results in columns 2 to 5, with which the existence of mixed parity superconductivity, the dominant pair potential and time-reversal symmetry breaking may be detected. The dominance of the order parameter can generally be extracted from column 2. The parameter r and the overall energy scale Δ_0 can then be estimated using the results in columns 3 and 4 via $\min(r,\frac{1}{r}) = \frac{eV_{\mathrm{ani,max}}-eV_{\mathrm{ani,min}}}{eV_{\mathrm{ani,max}}+eV_{\mathrm{ani,min}}}$ and $\Delta_0 = \frac{eV_{\mathrm{ani,max}}\sqrt{1+r^2}}{1+r}$ in the $s+$ helical p-wave case and $r = \sqrt{(\frac{eV_{\mathrm{ani,max}}}{eV_{\mathrm{ani,min}}})^2-1}$ with $\Delta_0 = eV_{\mathrm{ani,max}}$ in the $s+$ helical p-wave case, while the direction of $\langle \boldsymbol{d}\rangle$ may be extracted from column 6. We note from Fig. 5 that for $r\approx 1$ a Thouless peak may elevate $\sigma(eV=0)$ above σ_N as well, while the estimates for r become less accurate as well.

Type	$\sigma(eV=0,h=0)>\sigma_N$	$eV_{\mathrm{ani,min}}/\Delta_0$	$eV_{\mathrm{ani,max}}/\Delta_0$	$\sigma(h\neq 0)>\sigma(h=0)$	Maximization of conductance
s wave	No	–	–	No	–
p wave	Yes	–	–	No	–
$s+p$ wave, $r<1$	No	$\frac{1-r}{\sqrt{1+r^2}}$	$\frac{1+r}{\sqrt{1+r^2}}$	No	$\boldsymbol{h}\parallel\langle\boldsymbol{d}\rangle$
$s+p$ wave, $r>1$	Yes	$\frac{r-1}{\sqrt{1+r^2}}$	$\frac{r+1}{\sqrt{1+r^2}}$	No	$\boldsymbol{h}\parallel\langle\boldsymbol{d}\rangle$
$is+p$ wave, $r<1$	No	$\frac{1}{\sqrt{1+r^2}}$	1	Yes	$\boldsymbol{h}\perp\langle\boldsymbol{d}\rangle$
$is+p$ wave, $r>1$	Yes	$\frac{1}{\sqrt{1+r^2}}$	1	Yes	$\boldsymbol{h}\perp\langle\boldsymbol{d}\rangle$

can be understood by considering the phase difference for each mode, depicted in Fig. 8. For $(i)s+$ helical p-wave superconductors, the phase difference between the s-wave and helical p-wave components is 0 or $\pi/2$ for all modes. On the other hand, in the chiral case, the phase difference is mode dependent and therefore, for some modes, the differential conductance is enhanced, while for others it is suppressed. For $s+$ chiral p-wave superconductors, the phase difference ranges between $-\pi/2$ and $\pi/2$, whereas for $is+$ chiral p-wave superconductors, it ranges between $-\pi$ and 0. These two cases are still different because the transparency is higher for the mode at normal incidence compared to the modes at large angle incidences and hence, in the $is+$ chiral p-wave case, the modes contributing to the enhancement have a higher transparency compared to the $s+$ chiral p-wave case. However, the variation of the phase difference considerably softens the difference between $s+$ chiral p-wave and $is+$ chiral p-wave superconductors, explaining why the observed enhancement is much weaker for $(i)s+$ chiral p-wave superconductors than for $(i)s+$ helical p-wave superconductors.

On the other hand, the anisotropy in the magnetoresistance is relatively much stronger for $(i)s+$ chiral p-wave superconductors than for $(i)s+$ helical p-wave superconductors. Indeed, for the chiral p-wave superconductor, the direction of the d vector is independent of the direction of momenta, and therefore for all modes exchange field and d vector are either parallel or perpendicular, and therefore the distinction between parallel and perpendicular orientations is clearer. However, due to the much smaller magnetoresistance, the absolute anisotropy is smaller than for the $(i)s+$ helical p-wave superconductors.

The significant suppression of conductance for the $is+$ chiral p-wave superconductors in the voltage region $\frac{1-r}{\sqrt{1+r^2}} < |eV|/\Delta_0 < \frac{1}{\sqrt{1+r^2}}$ in Fig. 6(a) can also be understood using this picture. As discussed in the Sec. III on $(i)s+$ helical p-wave superconductors, the modes for which the phase difference between singlet and triplet components is $\pi/2$ enhance the differential conductance only for $\frac{1}{\sqrt{1+r^2}} < |eV|/\Delta_0 < 1$. On the other hand, for modes in which the phase difference between singlet and triplet components is almost 0, the differential conductance is suppressed in the larger window $\frac{1-r}{\sqrt{1+r^2}} < |eV|/\Delta_0 < \frac{1+r}{\sqrt{1+r^2}}$ [158]. Thus, for $\frac{1-r}{\sqrt{1+r^2}} < |eV|/\Delta_0 < \frac{1}{\sqrt{1+r^2}}$, the differential conductance is suppressed by an exchange field.

V. DISCUSSION

We have presented a method to determine the pair potential in time-reversal symmetry broken noncentrosymmetric $(i)s+$ p-wave superconductors. The differential conductance close to the gap edge is enhanced by an exchange field in the presence of time-reversal symmetry breaking in the superconductor. Next to this, our results show that by varying the direction of the exchange field, this enhancement can also be used to determine the direction of the d vector of the triplet correlations. With this, we have presented a theory for the complete determination of the pair potential in $(i)s+$ helical p-wave superconductors, as summarized in Table I. The mixing parameter, the phase difference between singlet and triplet components, and direction of the d vector can all be estimated from conductance measurements in SFN junctions. We note that the results in Table I do not depend on the specific choice of geometric parameters chosen in this paper, as confirmed in the Appendix.

Our results show that if the exchange field is small compared to the Fermi energy, the magnetoresistance of the SFN junction is quadrupolar, and hence qualitatively different from the dipolar giant magnetoresistance found if the ferromagnetic interaction is comparable to the Fermi energy. Indeed, we found that maximal enhancement is obtained in perpendicular exchange fields, while minima are achieved in both parallel and antiparallel orientations. On the other hand, giant magnetoresistance for $h/E_F\sim 1$ distinguishes between parallel and antiparallel orientations. The enhancement is only present in a

specific voltage window, determined by the mixing parameter, but can reach $0.1\sigma_N$.

To determine the pair potential in an arbitrary [193] time-reversal and inversion symmetry broken single band superconductor, one needs to also include other types of p waves and higher order angular momenta, d wave, f wave, etc. in the pair potential.

For such superconductors, the differential conductance is quantitatively different, but since the differential conductance enhancement depends only on the phase between the superconductors and the relative orientation of the spin in the superconductor and ferromagnet, the qualitative features of our results should also be visible in junctions with $(i)s + f$ or $(i)d + p$-wave superconductors, as long as the individual components do not break time-reversal symmetry, i.e., they are not chiral. For $(i)s +$ chiral p-wave superconductors, which may be distinguished from $(i)s +$ helical p-wave superconductors using the directional dependence of the d vector [158], the mode dependence of the phase difference smoothens the results and makes the extraction of the parameter r more difficult. However, χ_t may be determined using the differential conductance enhancement. The exact dependence of phase and d vector on the mode may be illuminated by using geometries in which a single superconductor participates in more than one junction, as proposed in Ref. [185]. The theory cannot be used for $s + id$ ($p + if$) superconductors, as in such superconductors only singlet (triplet) correlations are present.

The presented theory might be extended to include such higher order contributions to the pair potential or to add a spatially dependent exchange field in the ferromagnet. The latter is known to lead to long-range proximity effects [187,194]. Another interesting direction would be to include the time-reversal symmetry breaking or inversion symmetry breaking in the normal metal instead of the superconductor to describe the proximity effect in for example Weyl semimetals [195]. Such extension would require the derivation of the Usadel equations in those systems.

Results show that both regimes in which the exchange field is much stronger or weaker than the pair potential may be used to identify the pairing symmetry. In the former case, one may use conventional ferromagnets, which usually have a Curie temperature larger than the critical temperature of superconductors. For the latter case, we recommend either the use of normal metals proximized by a ferromagnetic insulator such as EuS or EuO from below or junctions in which the contact between the superconductor and the ferromagnet is weak, that is, the boundary resistance is high, $\gamma_B \gg \Delta/h$, so the ferromagnetic axis is not rotated by the spin-dependent density of states of the $is + p$-wave superconductor. In this parameter regime, self-consistency of the ferromagnetic interaction may be ignored. If the combination of weak ferromagnets such as has been observed in perovskites [196] and a strong coupling between the two materials is used, self-consistency of the ferromagnetic interaction cannot be ignored. Its inclusion does not lead to qualitative changes, but will lead to a suppression of the quadrupolar dependence of the magnetoresistance as the superconductor changes the direction of the exchange field. Therefore, the effect is harder to measure in this regime. Quantitative treatment of such effects is beyond the scope of this paper.

In both the strong and weak field cases, we recommend to use materials in which there are no strong preferential directions for the exchange field, so this direction can be rotated via application of external magnetic field and remains in the altered direction after switching this external field off. Next to this, for the use of the dirty limit Usadel equation, it is important to certify that the ferromagnet is not in the clean limit, that is, its normal state resistance should not be exceptionally low.

ACKNOWLEDGMENTS

We thank F. S. Bergeret for useful discussions. T.K. acknowledges financial support from Spanish MCIN/AEI/10.13039/501100011033 through Projects No. PID2020-114252GB-I00 (SPIRIT) and No. TED2021-130292B-C42, and the Basque Government through Grant No. IT-1591-22. Y.T. acknowledges support from JSPS with Grants-in-Aid for Scientific research (KAKENHI Grants No. 23K17668 and No. 24K00583).

APPENDIX: PARAMETER DEPENDENCE

To study the robustness of the quadrupolar enhancement of conductance in the presence of an exchange field, we repeated the calculations for different values of the parameters γ_B, z, E_{Th}, Δ_0 describing the geometry of the junction and $r = 2$. We consider the junction with an $is +$ helical p-wave superconductor. As shown in the figures below, even though the differential conductance strongly depends on the geometry of the junction, the enhancement is indeed robust against changes in these parameters—in all cases there is a strong enhancement of conductance in the range $\frac{1}{\sqrt{1+r^2}} < eV/\Delta_0 < 1$ if an exchange field is applied perpendicular to the angular averaged d-vector, while this effect is much smaller if the exchange field is applied parallel to the averaged d-vector.

The size of the effect may depend on the boundary resistance of the junction. As shown in Figs. 9 and 10, the effect is more apparent if the boundary resistance is lower, that is, if the proximity effect is stronger. Indeed, in this case the pair amplitudes are larger, which leads to larger suppression of the density of states and thus allows for a stronger spin dependence of the density of states.

Based on Figs. 11 and 12, we recommend using a relatively long junction, so the effects of the ZBCP can be best disentangled from the enhancement of conductance.

Indeed, if the length is increased, see Fig. 11, so the Thouless energy becomes smaller, the changes in the results are very small compared to those presented in the main text. On the other hand, if the length of the junction is decreased, as shown in Fig. 12, due to the increase in Thouless energy, the peak at $eV = h$ becomes less sharp than before and makes it more difficult to distinguish this peak from the enhancement of magnetoresistance due to the internal time-reversal symmetry breaking of the superconductor. However, there remains a region in which the differential conductance is enhanced by

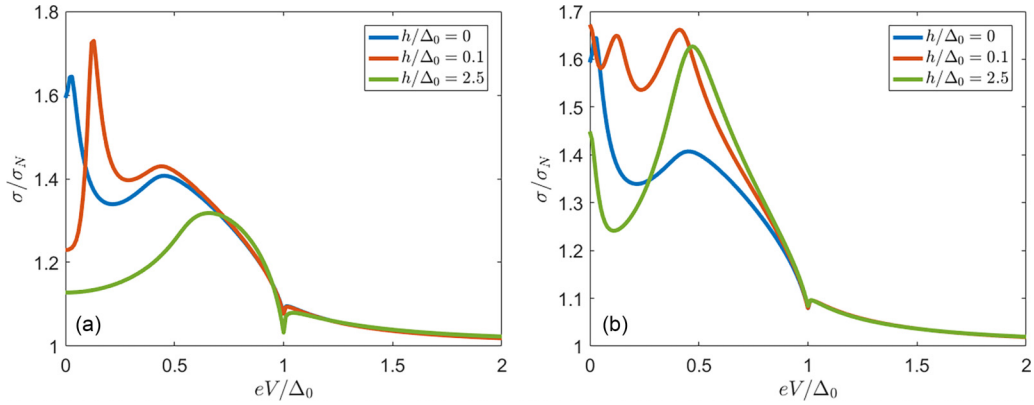

FIG. 9. The differential conductance of the is + helical p-wave junction with $r = 2$ for different exchange fields if the boundary resistance is lowered such that $\gamma_{BS} = 0.5$, with fields in the (a) parallel or (b) perpendicular orientation. In both orientations, there is an enhancement of conductance by an exchange field, which is larger in the perpendicular compared to the parallel orientation. This quadrupolar dependence can be used to distinguish the is + helical p-wave enhancement from the peak at $eV = h$. We recommend using $h > \Delta_0$ to avoid the latter effect.

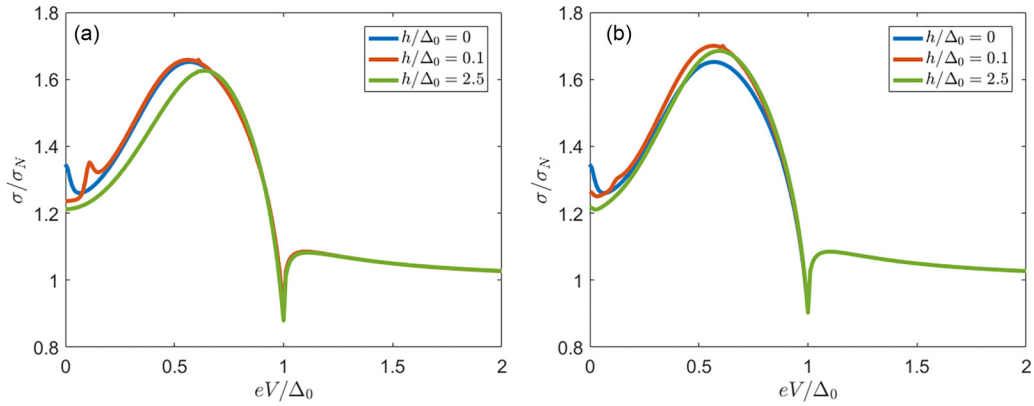

FIG. 10. The differential conductance of the is + helical p-wave junction with $r = 2$ for different exchange fields if the boundary resistance is enhanced such that $\gamma_{BS} = 5$, with fields in the (a) parallel or (b) perpendicular orientation. In the perpendicular orientation, there is a clear enhancement of conductance by an exchange field, while in the parallel orientation this effect is almost absent. The peak at $eV = h$ is small and hence does not play a role in this parameter regime.

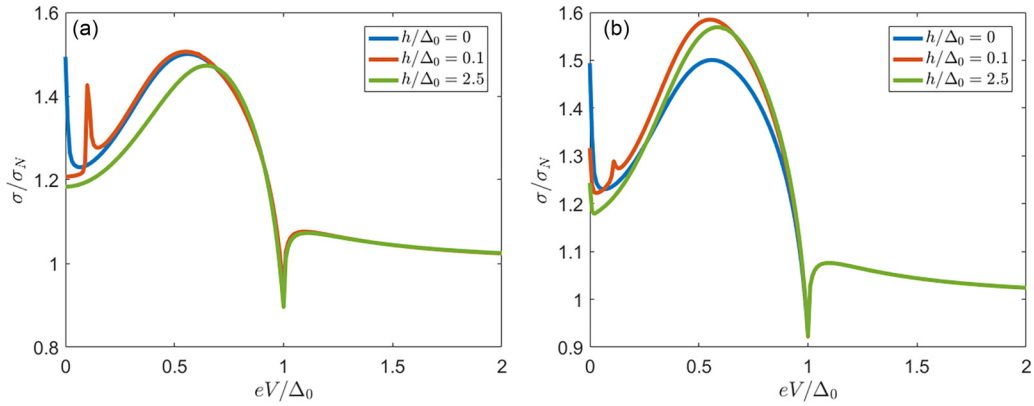

FIG. 11. The differential conductance of the is + helical p-wave junction with $r = 2$ for different exchange fields if the length is increased, so $E_{\mathrm{Th}}/\Delta_0 = 0.01$, with fields in the (a) parallel or (b) perpendicular orientation. In the perpendicular orientation, there is a clear enhancement of conductance by an exchange field; in the parallel orientation the enhancement is small. The peak at $eV = h$ is very sharp in this parameter regime, so the quadrupolar enhancement can be easily distinguished from this effect.

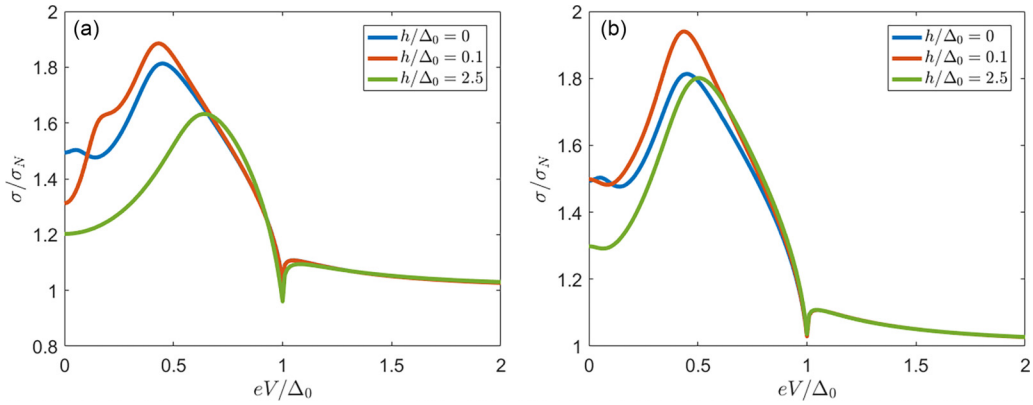

FIG. 12. The differential conductance of the is + helical p-wave junction with $r = 2$ for different exchange fields if the length is decreased, so $E_{\mathrm{Th}}/\Delta_0 = 0.04$, with fields in the (a) parallel or (b) perpendicular orientation. In both orientations, there is a clear enhancement. The peak at $eV = h$ is relatively broad. For this reason, we recommend using the regime $h > \Delta_0$ to disentangle the two effects.

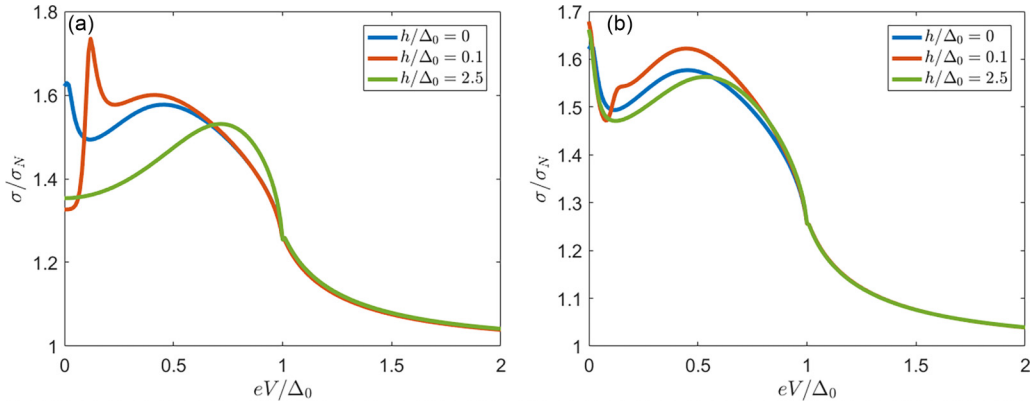

FIG. 13. The differential conductance of the is + helical p-wave junction with $r = 2$ for different exchange fields if the transparency is increased, so $z = 0.5$, with fields in the (a) parallel or (b) perpendicular orientation. In both orientations, there is a clear enhancement of conductance by an exchange field. It is harder to distinguish between the parallel and perpendicular orientations due to the similar contribution of modes with normal and oblique incidence.

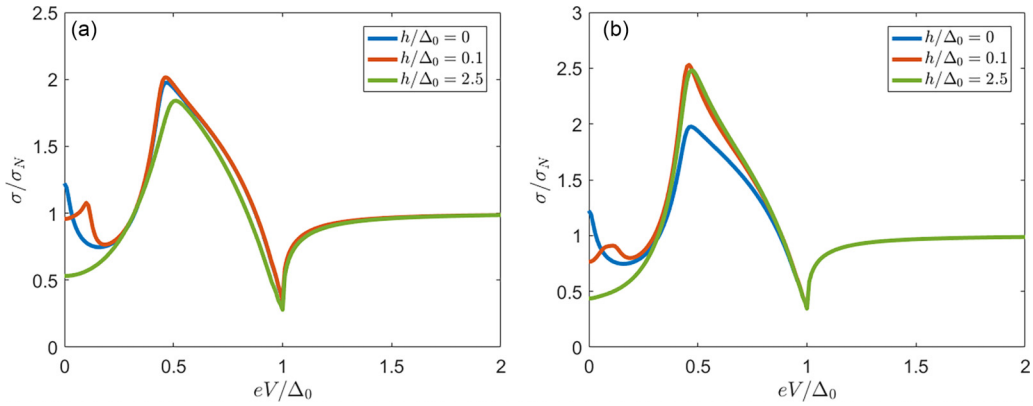

FIG. 14. The differential conductance of the is + helical p-wave junction with $r = 2$ for different exchange fields if the transparency is decreased, so $z = 2$, with fields in the (a) parallel or (b) perpendicular orientation. There is a clear difference between the perpendicular orientation and parallel orientation, with a large enhancement of conductance if $\boldsymbol{h}$ and $\langle \boldsymbol{d} \rangle$ are perpendicular that is almost absent if these two vectors are parallel.

application of an exchange field, and for small fields the width of the voltage window in which this effect appears does not change. Thus, the results remain qualitatively the same.

The parameter with the strongest influence on the differential conductance enhancement is the BTK parameter z. Indeed, if z becomes smaller, the transparency is enhanced, see Fig. 13, the differences in contributions of the mode normal to the interface and the ones with oblique incidence are smaller, and hence the difference in results for parallel and perpendicular fields becomes smaller, suppressing the quadrupolar conductance enhancement. If z is increased, that is, the transparency is decreased, see Fig. 14, the relative distinction between the parallel and perpendicular orientations becomes larger, that is, the quadrupolar enhancement is more clearly observable in measurement. The 1D limit, however, cannot be obtained by varying z. Indeed, if $z \gg 1$, $T(\phi) \propto \cos^2 \phi$, and therefore the oblique modes still contribute significantly compared to the mode with normal incidence.

[1] M. Sigrist and K. Ueda, Phenomenological theory of unconventional superconductivity, Rev. Mod. Phys. **63**, 239 (1991).

[2] A. P. Schnyder, S. Ryu, A. Furusaki, and A. W. W. Ludwig, Classification of topological insulators and superconductors in three spatial dimensions, Phys. Rev. B **78**, 195125 (2008).

[3] C. Kallin and A. Berlinsky, Is Sr_2RuO_4 a chiral p-wave superconductor? J. Phys.: Condens. Matter **21**, 164210 (2009).

[4] Y. Maeno, S. Kittaka, T. Nomura, S. Yonezawa, and K. Ishida, Evaluation of spin-triplet superconductivity in Sr_2RuO_4, J. Phys. Soc. Jpn. **81**, 011009 (2012).

[5] M. Sigrist, Review on the chiral p-wave phase of Sr_2RuO_4, Prog. Theor. Phys. Suppl. **160**, 1 (2005).

[6] A. P. Mackenzie, T. Scaffidi, C. W. Hicks, and Y. Maeno, Even odder after twenty-three years: the superconducting order parameter puzzle of Sr_2RuO_4, npj Quantum Mater. **2**, 40 (2017).

[7] C. Kallin and J. Berlinsky, Chiral superconductors, Rep. Prog. Phys. **79**, 054502 (2016).

[8] J. Linder and A. V. Balatsky, Odd-frequency superconductivity, Rev. Mod. Phys. **91**, 045005 (2019).

[9] R. Balian and N. Werthamer, Superconductivity with pairs in a relative p wave, Phys. Rev. **131**, 1553 (1963).

[10] L. Fu and C. L. Kane, Superconducting proximity effect and Majorana fermions at the surface of a topological insulator, Phys. Rev. Lett. **100**, 096407 (2008).

[11] S.-P. Chiu, C. Tsuei, S.-S. Yeh, F.-C. Zhang, S. Kirchner, and J.-J. Lin, Observation of triplet superconductivity in $CoSi_2/TiSi_2$ heterostructures, Sci. Adv. **7**, eabg6569 (2021).

[12] S.-P. Chiu, C.-J. Wang, Y.-C. Lin, S.-T. Tu, S. Sahu, R.-T. Wang, C.-Y. Wu, S.-S. Yeh, S. Kirchner, and J.-J. Lin, Electronic conduction and superconducting properties of $CoSi_2$ films on silicon–an unconventional superconductor with technological potential, arXiv:2401.17601.

[13] E. Bauer, G. Hilscher, H. Michor, C. Paul, E.-W. Scheidt, A. Gribanov, Y. Seropegin, H. Noël, M. Sigrist, and P. Rogl, Heavy fermion superconductivity and magnetic order in noncentrosymmetric $CePt_3Si$, Phys. Rev. Lett. **92**, 027003 (2004).

[14] J. Linder and J. W. Robinson, Superconducting spintronics, Nat. Phys. **11**, 307 (2015).

[15] H. G. Suh, H. Menke, P. M. R. Brydon, C. Timm, A. Ramires, and D. F. Agterberg, Stabilizing even-parity chiral superconductivity in Sr_2RuO_4, Phys. Rev. Res. **2**, 032023(R) (2020).

[16] D. Aoki, K. Ishida, and J. Flouquet, Review of U-based ferromagnetic superconductors: Comparison between UGe2, URhGe, and UCoGe, J. Phys. Soc. Jpn. **88**, 022001 (2019).

[17] S. Saxena, P. Agarwal, K. Ahilan, F. Grosche, R. Haselwimmer, M. Steiner, E. Pugh, I. Walker, S. Julian, P. Monthoux *et al.*, Superconductivity on the border of itinerant-electron ferromagnetism in UGe_2, Nature (London) **406**, 587 (2000).

[18] D. Aoki, A. Huxley, E. Ressouche, D. Braithwaite, J. Flouquet, J.-P. Brison, E. Lhotel, and C. Paulsen, Coexistence of superconductivity and ferromagnetism in URhGe, Nature (London) **413**, 613 (2001).

[19] F. Hardy and A. D. Huxley, p-wave superconductivity in the ferromagnetic superconductor URhGe, Phys. Rev. Lett. **94**, 247006 (2005).

[20] N. T. Huy, A. Gasparini, D. E. de Nijs, Y. Huang, J. C. P. Klaasse, T. Gortenmulder, A. de Visser, A. Hamann, T. Görlach, and H. v. Löhneysen, Superconductivity on the border of weak itinerant ferromagnetism in UCoGe, Phys. Rev. Lett. **99**, 067006 (2007).

[21] S. Ran, C. Eckberg, Q.-P. Ding, Y. Furukawa, T. Metz, S. R. Saha, I.-L. Liu, M. Zic, H. Kim, J. Paglione *et al.*, Nearly ferromagnetic spin-triplet superconductivity, Science **365**, 684 (2019).

[22] J. Yang, J. Luo, C. Yi, Y. Shi, Y. Zhou, and G.-q. Zheng, Spin-triplet superconductivity in $K_2Cr_3As_3$, Sci. Adv. **7**, eabl4432 (2021).

[23] Y. Tanaka and S. Kashiwaya, Anomalous charge transport in triplet superconductor junctions, Phys. Rev. B **70**, 012507 (2004).

[24] Y. Tanaka, S. Kashiwaya, and T. Yokoyama, Theory of enhanced proximity effect by midgap Andreev resonant state in diffusive normal-metal/triplet superconductor junctions, Phys. Rev. B **71**, 094513 (2005).

[25] S.-I. Suzuki, T. Hirai, M. Eschrig, and Y. Tanaka, Anomalous inverse proximity effect in unconventional superconductor junctions, Phys. Rev. Res. **3**, 043148 (2021).

[26] V. Berezinskii, New model of the anisotropic phase of superfluid He_3, Pis'ma Zh. Eksp. Teor. Fiz. **20**, 628 (1974) [JETP Lett. **20**, 287 (1974)].

[27] A. Balatsky and E. Abrahams, New class of singlet superconductors which break the time reversal and parity, Phys. Rev. B **45**, 13125 (1992).

[28] D. Belitz and T. R. Kirkpatrick, Even-parity spin-triplet superconductivity in disordered electronic systems, Phys. Rev. B **46**, 8393 (1992).

[29] E. Abrahams, A. Balatsky, D. J. Scalapino, and J. R. Schrieffer, Properties of odd-gap superconductors, Phys. Rev. B **52**, 1271 (1995).

[30] T. R. Kirkpatrick and D. Belitz, Disorder-induced triplet superconductivity, Phys. Rev. Lett. **66**, 1533 (1991).

[31] P. Coleman, A. Georges, and A. Tsvelik, Reflections on the one-dimensional realization of odd-frequency pairing, J. Phys.: Condens. Matter **9**, 345 (1997).

[32] J. Cayao, C. Triola, and A. M. Black-Schaffer, Odd-frequency superconducting pairing in one-dimensional systems, Eur. Phys. J.: Spec. Top. **229**, 545 (2020).

[33] P. Gentile, C. Noce, A. Romano, G. Annunziata, J. Linder, and M. Cuoco, Odd-frequency triplet pairing in mixed-parity superconductors, arXiv:1109.4885.

[34] Y. Tanaka and A. A. Golubov, Theory of the proximity effect in junctions with unconventional superconductors, Phys. Rev. Lett. **98**, 037003 (2007).

[35] Y. Tanaka, M. Sato, and N. Nagaosa, Symmetry and topology in superconductors–odd-frequency pairing and edge states–, J. Phys. Soc. Jpn. **81**, 011013 (2012).

[36] A. Tsintzis, A. M. Black-Schaffer, and J. Cayao, Odd-frequency superconducting pairing in Kitaev-based junctions, Phys. Rev. B **100**, 115433 (2019).

[37] D. Kuzmanovski, A. M. Black-Schaffer, and J. Cayao, Suppression of odd-frequency pairing by phase disorder in a nanowire coupled to Majorana zero modes, Phys. Rev. B **101**, 094506 (2020).

[38] F. Wenger and S. Östlund, d-wave pairing in tetragonal superconductors, Phys. Rev. B **47**, 5977 (1993).

[39] D. S. Rokhsar, Pairing in doped spin liquids: Anyon versus d-wave superconductivity, Phys. Rev. Lett. **70**, 493 (1993).

[40] M. Covington, M. Aprili, E. Paraoanu, L. H. Greene, F. Xu, J. Zhu, and C. A. Mirkin, Observation of surface-induced broken time-reversal symmetry in $YBa_2Cu_3O_7$ tunnel junctions, Phys. Rev. Lett. **79**, 277 (1997).

[41] M. Sigrist, N. Ogawa, and K. Ueda, Phenomenology of an unconventional superconductor in a thin film, Physica C: Superconductivity **185-189**, 2053 (1991).

[42] R. Laughlin, Tunneling gap as evidence for time-reversal symmetry breaking at surfaces of high-temperature superconductors, Physica C: Superconductivity **234**, 280 (1994).

[43] R. B. Laughlin, Magnetic induction of $d_{x^2-y^2} + \mathrm{id}_{xy}$ order in High- T_c superconductors, Phys. Rev. Lett. **80**, 5188 (1998).

[44] A. D. Hillier, J. Quintanilla, and R. Cywinski, Evidence for time-reversal symmetry breaking in the noncentrosymmetric superconductor $LaNiC_2$, Phys. Rev. Lett. **102**, 117007 (2009).

[45] R. Wakatsuki, Y. Saito, S. Hoshino, Y. M. Itahashi, T. Ideue, M. Ezawa, Y. Iwasa, and N. Nagaosa, Nonreciprocal charge transport in noncentrosymmetric superconductors, Sci. Adv. **3**, e1602390 (2017).

[46] S. A. Kivelson, A. C. Yuan, B. Ramshaw, and R. Thomale, A proposal for reconciling diverse experiments on the superconducting state in Sr_2RuO_4, npj Quantum Mater. **5**, 43 (2020).

[47] J. Xia, Y. Maeno, P. T. Beyersdorf, M. M. Fejer, and A. Kapitulnik, High resolution polar kerr effect measurements of Sr_2RuO_4: Evidence for broken time-reversal symmetry in the superconducting state, Phys. Rev. Lett. **97**, 167002 (2006).

[48] G. M. Luke, Y. Fudamoto, K. Kojima, M. Larkin, J. Merrin, B. Nachumi, Y. Uemura, Y. Maeno, Z. Mao, Y. Mori *et al.*, Time-reversal symmetry-breaking superconductivity in Sr_2RuO_4, Nature (London) **394**, 558 (1998).

[49] J. Clepkens, A. W. Lindquist, and H.-Y. Kee, Shadowed triplet pairings in Hund's metals with spin-orbit coupling, Phys. Rev. Res. **3**, 013001 (2021).

[50] M. Sigrist, Time-reversal symmetry breaking states in high-temperature superconductors, Prog. Theor. Phys. **99**, 899 (1998).

[51] S. K. Ghosh, M. Smidman, T. Shang, J. F. Annett, A. D. Hillier, J. Quintanilla, and H. Yuan, Recent progress on superconductors with time-reversal symmetry breaking, J. Phys.: Condens. Matter **33**, 033001 (2020).

[52] S. K. Ghosh, P. K. Biswas, C. Xu, B. Li, J. Z. Zhao, A. D. Hillier, and X. Xu, Time-reversal symmetry breaking superconductivity in three-dimensional Dirac semimetallic silicides, Phys. Rev. Res. **4**, L012031 (2022).

[53] W.-C. Lee, S.-C. Zhang, and C. Wu, Pairing state with a time-reversal symmetry breaking in FeAs-based superconductors, Phys. Rev. Lett. **102**, 217002 (2009).

[54] C. Farhang, N. Zaki, J. Wang, G. Gu, P. D. Johnson, and J. Xia, Revealing the origin of time-reversal symmetry breaking in Fe-chalcogenide superconductor $FeTe_{1-x}Se_x$, Phys. Rev. Lett. **130**, 046702 (2023).

[55] M. O. Ajeesh, M. Bordelon, C. Girod, S. Mishra, F. Ronning, E. D. Bauer, B. Maiorov, J. D. Thompson, P. F. S. Rosa, and S. M. Thomas, Fate of time-reversal symmetry breaking in UTe_2, Phys. Rev. X **13**, 041019 (2023).

[56] T. Shang, M. Smidman, A. Wang, L.-J. Chang, C. Baines, M. K. Lee, Z. Y. Nie, G. M. Pang, W. Xie, W. B. Jiang, M. Shi, M. Medarde, T. Shiroka, and H. Q. Yuan, Simultaneous nodal superconductivity and time-reversal symmetry breaking in the noncentrosymmetric superconductor CaPtAs, Phys. Rev. Lett. **124**, 207001 (2020).

[57] V. Grinenko, S. Ghosh, R. Sarkar, J.-C. Orain, A. Nikitin, M. Elender, D. Das, Z. Guguchia, F. Brückner, M. E. Barber *et al.*, Split superconducting and time-reversal symmetry-breaking transitions in Sr_2RuO_4 under stress, Nat. Phys. **17**, 748 (2021).

[58] R. Willa, M. Hecker, R. M. Fernandes, and J. Schmalian, Inhomogeneous time-reversal symmetry breaking in Sr_2RuO_4, Phys. Rev. B **104**, 024511 (2021).

[59] A. Maisuradze, W. Schnelle, R. Khasanov, R. Gumeniuk, M. Nicklas, H. Rosner, A. Leithe-Jasper, Y. Grin, A. Amato, and P. Thalmeier, Evidence for time-reversal symmetry breaking in superconducting $PrPt_4Ge_{12}$, Phys. Rev. B **82**, 024524 (2010).

[60] H. S. Røising, G. Wagner, M. Roig, A. T. Rømer, and B. M. Andersen, Heat capacity double transitions in time-reversal symmetry broken superconductors, Phys. Rev. B **106**, 174518 (2022).

[61] R. Movshovich, M. Jaime, M. Hubbard, M. Salamon, A. Balatsky, R. Yoshizaki, and J. Sarrao, Low-temperature phase transition in $Bi_2Sr_2Ca(Cu_{1-x}Ni_x)_2O_8$, J. Phys. Chem. Solids **59**, 2100 (1998).

[62] A. Balatsky, Spontaneous time reversal and parity breaking in a d_{x2-y2}-wave superconductor with magnetic impurities, J. Phys. Chem. Solids **59**, 1689 (1998).

[63] V. Belyavsky, V. Kapaev, and Y. V. Kopaev, Chiral d-wave superconductor with nonzero center-of-mass pair momentum, arXiv:1209.0884.

[64] A. M. Black-Schaffer and C. Honerkamp, Chiral d-wave superconductivity in doped graphene, J. Phys.: Condens. Matter **26**, 423201 (2014).

[65] Y. Tanaka, Y. Tanuma, and S. Kashiwaya, Influence of impurity scattering on tunneling conductance in normal-metal–d-wave superconductor junctions, Phys. Rev. B **64**, 054510 (2001).

[66] M. Sigrist, D. B. Bailey, and R. B. Laughlin, Fractional vortices as evidence of time-reversal symmetry breaking in high-temperature superconductors, Phys. Rev. Lett. **74**, 3249 (1995).

[67] M. Palumbo, P. Muzikar, and J. A. Sauls, Magnetic instabilities in unconventional superconductors, Phys. Rev. B **42**, 2681 (1990).

[68] K. Kuboki and M. Sigrist, Proximity-induced time-reversal symmetry breaking at Josephson junctions between unconventional superconductors, J. Phys. Soc. Jpn. **65**, 361 (1996).

[69] Y. Tanuma, Y. Tanaka, M. Ogata, and S. Kashiwaya, Quasiparticle states near surfaces of high$-T_c$ superconductors based on the extended $t-J$ model, Phys. Rev. B **60**, 9817 (1999).

[70] Y. Tanuma, Y. Tanaka, and S. Kashiwaya, Tunneling conductance of normal metal/$d_{x^2-y^2}$-wave superconductor junctions in the presence of broken time-reversal symmetry states near interfaces, Phys. Rev. B **64**, 214519 (2001).

[71] M. Fogelström, D. Rainer, and J. A. Sauls, Tunneling into current-carrying surface states of high- T_C superconductors, Phys. Rev. Lett. **79**, 281 (1997).

[72] R. Krupke and G. Deutscher, Anisotropic magnetic field dependence of the zero-bias anomaly on in-plane oriented [100] $Y_1Ba_2Cu_3O_{7-x}$/In tunnel junctions, Phys. Rev. Lett. **83**, 4634 (1999).

[73] M. Matsumoto and H. Shiba, Coexistence of different symmetry order parameters near a surface in d-wave superconductors II, J. Phys. Soc. Jpn. **64**, 4867 (1995).

[74] B. M. Andersen, A. Kreisel, and P. Hirschfeld, Spontaneous time-reversal symmetry breaking by disorder in superconductors, arXiv:2312.08099.

[75] G. Amano, S. Akutagawa, T. Muranaka, Y. Zenitani, and J. Akimitsu, Superconductivity at 18 K in yttrium sesquicarbide system, Y_2C_3, J. Phys. Soc. Jpn. **73**, 530 (2004).

[76] T. Akazawa, H. Hidaka, H. Kotegawa, T. C. Kobayashi, T. Fujiwara, E. Yamamoto, Y. Haga, R. Settai, and Y. Ōnuki, Pressure-induced superconductivity in UIr, J. Phys. Soc. Jpn. **73**, 3129 (2004).

[77] K. Togano, P. Badica, Y. Nakamori, S. Orimo, H. Takeya, and K. Hirata, Superconductivity in the metal rich Li-Pd-B ternary boride, Phys. Rev. Lett. **93**, 247004 (2004).

[78] N. Tateiwa, Y. Haga, T. D. Matsuda, S. Ikeda, T. Yasuda, T. Takeuchi, R. Settai, and Y. Ōnuki, Novel pressure phase diagram of heavy fermion superconductor $CePt_3Si$ investigated by ac calorimetry, J. Phys. Soc. Jpn. **74**, 1903 (2005).

[79] N. Kimura, K. Ito, K. Saitoh, Y. Umeda, H. Aoki, and T. Terashima, Pressure-induced superconductivity in noncentrosymmetric heavy-fermion $CeRhSi_3$, Phys. Rev. Lett. **95**, 247004 (2005).

[80] I. Sugitani, Y. Okuda, H. Shishido, T. Yamada, A. Thamizhavel, E. Yamamoto, T. D. Matsuda, Y. Haga, T. Takeuchi, R. Settai *et al.*, Pressure-induced heavy-fermion superconductivity in antiferromagnet $CeIrSi_3$ without inversion symmetry, J. Phys. Soc. Jpn. **75**, 043703 (2006).

[81] F. Honda, I. Bonalde, K. Shimizu, S. Yoshiuchi, Y. Hirose, T. Nakamura, R. Settai, and Y. Ōnuki, Pressure-induced superconductivity and large upper critical field in the noncentrosymmetric antiferromagnet $CeIrGe_3$, Phys. Rev. B **81**, 140507(R) (2010).

[82] R. Settai, I. Sugitani, Y. Okuda, A. Thamizhavel, M. Nakashima, Y. Ōnuki, and H. Harima, Pressure-induced superconductivity in $CeCoGe_3$ without inversion symmetry, J. Magn. Magn. Mater. **310**, 844 (2007), Proceedings of the 17th International Conference on Magnetism.

[83] E. Bauer, G. Rogl, X.-Q. Chen, R. T. Khan, H. Michor, G. Hilscher, E. Royanian, K. Kumagai, D. Z. Li, Y. Y. Li, R. Podloucky, and P. Rogl, Unconventional superconducting phase in the weakly correlated noncentrosymmetric Mo_3Al_2C compound, Phys. Rev. B **82**, 064511 (2010).

[84] W. Xie, P. Zhang, B. Shen, W. Jiang, G. Pang, T. Shang, C. Cao, M. Smidman, and H. Yuan, CaPtAs: A new noncentrosymmetric superconductor, Sci. China Math. **63**, 237412 (2020).

[85] M. Eschrig, C. Iniotakis, and Y. Tanaka, Properties of interfaces and surfaces in non-centrosymmetric superconductors, in *Non-Centrosymmetric Superconductors: Introduction and Overview*, edited by E. Bauer and M. Sigrist (Springer, Berlin, 2012), pp. 313–357.

[86] S. Matsubara, Y. Tanaka, and H. Kontani, Generation of odd-frequency surface superconductivity with spontaneous spin current due to the zero-energy Andreev bound state, Phys. Rev. B **103**, 245138 (2021).

[87] Y. Tanaka, T. Kokkeler, and A. Golubov, Theory of proximity effect in $s+p$-wave superconductor junctions, Phys. Rev. B **105**, 214512 (2022).

[88] S.-I. Suzuki, S. Ikegaya, and A. A. Golubov, Destruction of surface states of $(d_{zx}+id_{yz})$-wave superconductor by surface roughness: Application to Sr_2RuO_4, Phys. Rev. Res. **4**, L042020 (2022).

[89] S. Kanasugi and Y. Yanase, Anapole superconductivity from $\mathcal{PT}$-symmetric mixed-parity interband pairing, Commun. Phys. **5**, 39 (2022).

[90] T. Kitamura, S. Kanasugi, M. Chazono, and Y. Yanase, Quantum geometry induced anapole superconductivity, Phys. Rev. B **107**, 214513 (2023).

[91] M. Chazono, S. Kanasugi, T. Kitamura, and Y. Yanase, Piezoelectric effect and diode effect in anapole and monopole superconductors, Phys. Rev. B **107**, 214512 (2023).

[92] P. Goswami and B. Roy, Axionic superconductivity in three-dimensional doped narrow-gap semiconductors, Phys. Rev. B **90**, 041301(R) (2014).

[93] D. Möckli and M. Khodas, Magnetic-field induced $s+if$ pairing in Ising superconductors, Phys. Rev. B **99**, 180505(R) (2019).

[94] Y. Takabatake, S.-I. Suzuki, and Y. Tanaka, Tunneling conductance of the $(d+ip)$-wave superconductor, Phys. Rev. B **103**, 184515 (2021).

[95] S. Mishra, Y. Liu, E. D. Bauer, F. Ronning, and S. M. Thomas, Anisotropic magnetotransport properties of the heavy-fermion superconductor $CeRh_2As_2$, Phys. Rev. B **106**, L140502 (2022).

[96] Z. Wu, Y. Fang, H. Su, W. Xie, P. Li, Y. Wu, Y. Huang, D. Shen, B. Thiagarajan, J. Adell, C. Cao, H. Yuan, F. Steglich, and Y. Liu, Revealing the heavy quasiparticles in the heavy-fermion superconductor $CeCu_2Si_2$, Phys. Rev. Lett. **127**, 067002 (2021).

[97] F. S. Bergeret, A. F. Volkov, and K. B. Efetov, Induced ferromagnetism due to superconductivity in superconductor-ferromagnet structures, Phys. Rev. B **69**, 174504 (2004).

[98] C. Iniotakis, N. Hayashi, Y. Sawa, T. Yokoyama, U. May, Y. Tanaka, and M. Sigrist, Andreev bound states and tunneling characteristics of a noncentrosymmetric superconductor, Phys. Rev. B **76**, 012501 (2007).

[99] G. Annunziata, D. Manske, and J. Linder, Proximity effect with noncentrosymmetric superconductors, Phys. Rev. B **86**, 174514 (2012).

[100] Y. Rahnavard, D. Manske, and G. Annunziata, Magnetic Josephson junctions with noncentrosymmetric superconductors, Phys. Rev. B **89**, 214501 (2014).

[101] V. Mishra, Y. Li, F.-C. Zhang, and S. Kirchner, Effects of spin-orbit coupling in superconducting proximity devices: Application to $CoSi_2/TiSi_2$ heterostructures, Phys. Rev. B **103**, 184505 (2021).

[102] S. Ikegaya, S.-I. Suzuki, Y. Tanaka, and D. Manske, Proposal for identifying possible even-parity superconducting states in Sr_2RuO_4 using planar tunneling spectroscopy, Phys. Rev. Res. **3**, L032062 (2021).

[103] A. Daido and Y. Yanase, Majorana flat bands, chiral Majorana edge states, and unidirectional Majorana edge states in noncentrosymmetric superconductors, Phys. Rev. B **95**, 134507 (2017).

[104] S.-P. Chiu, V. Mishra, Y. Li, F.-C. Zhang, S. Kirchner, and J.-J. Lin, Tuning interfacial two-component superconductivity in $CoSi_2/TiSi_2$ heterojunctions via $TiSi_2$ diffusivity, Nanoscale **15**, 9179 (2023).

[105] K. Ishihara, T. Takenaka, Y. Miao, Y. Mizukami, K. Hashimoto, M. Yamashita, M. Konczykowski, R. Masuki, M. Hirayama, T. Nomoto, R. Arita, O. Pavlosiuk, P. Wiśniewski, D. Kaczorowski, and T. Shibauchi, Tuning the parity mixing of singlet-septet pairing in a half-Heusler superconductor, Phys. Rev. X **11**, 041048 (2021).

[106] T. Kokkeler, A. Golubov, S. Bergeret, and Y. Tanaka, Proximity effect of time-reversal symmetry broken noncentrosymmetric superconductors, Phys. Rev. B **108**, 094503 (2023).

[107] M. A. Silaev, I. V. Tokatly, and F. S. Bergeret, Anomalous current in diffusive ferromagnetic Josephson junctions, Phys. Rev. B **95**, 184508 (2017).

[108] Y. Zhang, Y. Gu, P. Li, J. Hu, and K. Jiang, General theory of Josephson diodes, Phys. Rev. X **12**, 041013 (2022).

[109] R. Wakatsuki and N. Nagaosa, Nonreciprocal current in noncentrosymmetric Rashba superconductors, Phys. Rev. Lett. **121**, 026601 (2018).

[110] F. Ando, Y. Miyasaka, T. Li, J. Ishizuka, T. Arakawa, Y. Shiota, T. Moriyama, Y. Yanase, and T. Ono, Observation of superconducting diode effect, Nature (London) **584**, 373 (2020).

[111] B. Pal, A. Chakraborty, P. K. Sivakumar, M. Davydova, A. K. Gopi, A. K. Pandeya, J. A. Krieger, Y. Zhang, S. Ju, N. Yuan *et al.*, Josephson diode effect from Cooper pair momentum in a topological semimetal, Nat. Phys. **18**, 1228 (2022).

[112] C. Baumgartner, L. Fuchs, A. Costa, S. Reinhardt, S. Gronin, G. C. Gardner, T. Lindemann, M. J. Manfra, P. E. Faria Junior, D. Kochan *et al.*, Supercurrent rectification and magnetochiral effects in symmetric Josephson junctions, Nat. Nanotechnol. **17**, 39 (2022).

[113] Y. Hou, F. Nichele, H. Chi, A. Lodesani, Y. Wu, M. F. Ritter, D. Z. Haxell, M. Davydova, S. Ilić, O. Glezakou-Elbert, A. Varambally, F. S. Bergeret, A. Kamra, L. Fu, P. A. Lee, and J. S. Moodera, Ubiquitous Superconducting diode effect in superconductor thin films, Phys. Rev. Lett. **131**, 027001 (2023).

[114] J.-X. Lin, P. Siriviboon, H. D. Scammell, S. Liu, D. Rhodes, K. Watanabe, T. Taniguchi, J. Hone, M. S. Scheurer, and J. Li, Zero-field superconducting diode effect in small-twist-angle trilayer graphene, Nat. Phys. **18**, 1221 (2022).

[115] Y.-Y. Lyu, J. Jiang, Y.-L. Wang, Z.-L. Xiao, S. Dong, Q.-H. Chen, M. V. Milošević, H. Wang, R. Divan, J. E. Pearson *et al.*, Superconducting diode effect via conformal-mapped nanoholes, Nat. Commun. **12**, 2703 (2021).

[116] H. Wu, Y. Wang, P. K. Sivakumar, C. Pasco, S. S. Parkin, Y.-J. Zeng, T. McQueen, and M. N. Ali, Realization of the field-free Josephson diode, Nature (London) **604**, 653 (2022).

[117] M. Silaev, A. Y. Aladyshkin, M. Silaeva, and A. Aladyshkina, The diode effect induced by domain-wall superconductivity, J. Phys.: Condens. Matter **26**, 095702 (2014).

[118] N. F. Yuan and L. Fu, Supercurrent diode effect and finite-momentum superconductors, Proc. Natl. Acad. Sci. USA **119**, e2119548119 (2022).

[119] S. Pal and C. Benjamin, Quantized Josephson phase battery, EPL (Europhysics Letters) **126**, 57002 (2019).

[120] W. Mayer, M. C. Dartiailh, J. Yuan, K. S. Wickramasinghe, E. Rossi, and J. Shabani, Gate controlled anomalous phase shift in Al/InAs Josephson junctions, Nat. Commun. **11**, 212 (2020).

[121] L. Bauriedl, C. Bäuml, L. Fuchs, C. Baumgartner, N. Paulik, J. M. Bauer, K.-Q. Lin, J. M. Lupton, T. Taniguchi, K. Watanabe *et al.*, Supercurrent diode effect and magnetochiral anisotropy in few-layer $NbSe_2$, Nat. Commun. **13**, 4266 (2022).

[122] A. A. Kopasov, A. G. Kutlin, and A. S. Mel'nikov, Geometry controlled superconducting diode and anomalous Josephson effect triggered by the topological phase transition in curved proximitized nanowires, Phys. Rev. B **103**, 144520 (2021).

[123] I. Margaris, V. Paltoglou, and N. Flytzanis, Zero phase difference supercurrent in ferromagnetic Josephson junctions, J. Phys.: Condens. Matter **22**, 445701 (2010).

[124] C.-Z. Chen, J. J. He, M. N. Ali, G.-H. Lee, K. C. Fong, and K. T. Law, Asymmetric Josephson effect in inversion symmetry breaking topological materials, Phys. Rev. B **98**, 075430 (2018).

[125] J. J. He, Y. Tanaka, and N. Nagaosa, A phenomenological theory of superconductor diodes, New J. Phys. **24**, 053014 (2022).

[126] T. H. Kokkeler, A. A. Golubov, and F. S. Bergeret, Field-free anomalous junction and superconducting diode effect in spin-split superconductor/topological insulator junctions, Phys. Rev. B **106**, 214504 (2022).

[127] T. Karabassov, E. S. Amirov, I. V. Bobkova, A. A. Golubov, E. A. Kazakova, and A. S. Vasenko, Superconducting diode effect in topological hybrid structures, Condensed Matter **8**, 36 (2023).

[128] T. de Picoli, Z. Blood, Y. Lyanda-Geller, and J. I. Väyrynen, Superconducting diode effect in quasi-one-dimensional systems, Phys. Rev. B **107**, 224518 (2023).

[129] S. Banerjee and M. S. Scheurer, Enhanced superconducting diode effect due to coexisting phases, Phys. Rev. Lett. **132**, 046003 (2024).

[130] J. J. Cuozzo, W. Pan, J. Shabani, and E. Rossi, Microwave-tunable diode effect in asymmetric SQUIDs with topological Josephson junctions, Phys. Rev. Res. **6**, 023011 (2024).

[131] L. Vigliotti, F. Cavaliere, G. Passetti, M. Sassetti, and N. T. Ziani, Reconstruction-induced ϕ_0 Josephson effect in quantum spin Hall constrictions, Nanomater. **13**, 1497 (2023).

[132] S. Ilić and F. S. Bergeret, Theory of the supercurrent diode effect in Rashba superconductors with arbitrary disorder, Phys. Rev. Lett. **128**, 177001 (2022).

[133] S. Ilić, P. Virtanen, T. T. Heikkilä, and F. S. Bergeret, Current rectification in junctions with spin-split superconductors, Phys. Rev. Appl. **17**, 034049 (2022).

[134] R. S. Souto, M. Leijnse, and C. Schrade, Josephson diode effect in supercurrent interferometers, Phys. Rev. Lett. **129**, 267702 (2022).

[135] J. J. He, Y. Tanaka, and N. Nagaosa, The supercurrent diode effect and nonreciprocal paraconductivity due to the chiral structure of nanotubes, Nat. Commun. **14**, 3330 (2023).

[136] A. Maiani, K. Flensberg, M. Leijnse, C. Schrade, S. Vaitiekėnas, and R. Seoane Souto, Nonsinusoidal current-phase relations in semiconductor–superconductor-ferromagnetic insulator devices, Phys. Rev. B **107**, 245415 (2023).

[137] A. Zazunov, J. Rech, T. Jonckheere, B. Grémaud, T. Martin, and R. Egger, Approaching ideal rectification in superconducting diodes through multiple Andreev reflections, arXiv:2307.14698.

[138] M. Nadeem, M. S. Fuhrer, and X. Wang, Superconducting diode effect–fundamental concepts, material aspects, and device prospects, arXiv:2301.13564.

[139] Y. Lu, I. V. Tokatly, and F. S. Bergeret, Ferromagnetic ordering of magnetic impurities mediated by supercurrents in the presence of spin-orbit coupling, Phys. Rev. B **108**, L180506 (2023).

[140] B. Lu, S. Ikegaya, P. Burset, Y. Tanaka, and N. Nagaosa, Tunable Josephson diode effect on the surface of topological insulators, Phys. Rev. Lett. **131**, 096001 (2023).

[141] A. Costa, J. Fabian, and D. Kochan, Microscopic study of the Josephson supercurrent diode effect inJosephson junctions based on two-dimensional electron gas, Phys. Rev. B **108**, 054522 (2023).

[142] M. Davydova, S. Prembabu, and L. Fu, Universal Josephson diode effect, Sci. Adv. **8**, eabo0309 (2022).

[143] T. Karabassov, I. V. Bobkova, A. A. Golubov, and A. S. Vasenko, Hybrid helical state and superconducting diode effect in superconductor/ferromagnet/topological insulator heterostructures, Phys. Rev. B **106**, 224509 (2022).

[144] F. Dolcini, M. Houzet, and J. S. Meyer, Topological Josephson ϕ_0 junctions, Phys. Rev. B **92**, 035428 (2015).

[145] A. Daido, Y. Ikeda, and Y. Yanase, Intrinsic superconducting diode effect, Phys. Rev. Lett. **128**, 037001 (2022).

[146] C. Ciaccia, R. Haller, A. C. C. Drachmann, T. Lindemann, M. J. Manfra, C. Schrade, and C. Schönenberger, Gate-tunable Josephson diode in proximitized InAs supercurrent interferometers, Phys. Rev. Res. **5**, 033131 (2023).

[147] X. Song, S. Suresh Babu, Y. Bai, D. S. Golubev, I. Burkova, A. Romanov, E. Ilin, J. N. Eckstein, and A. Bezryadin, Interference, diffraction, and diode effects in superconducting array based on bismuth antimony telluride topological insulator, Commun. Phys. **6**, 177 (2023).

[148] T. Kokkeler, I. Tokatly, and S. Bergeret, Nonreciprocal superconducting transport and the spin Hall effect in gyrotropic structures, SciPost Phys. **16**, 055 (2024).

[149] Y. Tanaka, B. Lu, and N. Nagaosa, Theory of giant diode effect in d-wave superconductor junctions on the surface of a topological insulator, Phys. Rev. B **106**, 214524 (2022).

[150] Y. Asano and S. Yamano, Josephson effect in noncentrosymmetric superconductor junctions, Phys. Rev. B **84**, 064526 (2011).

[151] L. Klam, A. Epp, W. Chen, M. Sigrist, and D. Manske, Josephson effect and triplet-singlet ratio of noncentrosymmetric superconductors, Phys. Rev. B **89**, 174505 (2014).

[152] S. Wu and K. V. Samokhin, Tunneling conductance of ferromagnet/noncentrosymmetric superconductor junctions, Phys. Rev. B **80**, 014516 (2009).

[153] S. Fujimoto, Unambiguous probe of parity mixing of Cooper pairs in noncentrosymmetric superconductors, Phys. Rev. B **79**, 220506(R) (2009).

[154] K. Børkje and A. Sudbø, Tunneling between noncentrosymmetric superconductors with significant spin-orbit splitting studied theoretically within a two-band treatment, Phys. Rev. B **74**, 054506 (2006).

[155] Y. Tanaka, Y. Mizuno, T. Yokoyama, K. Yada, and M. Sato, Anomalous Andreev bound state in noncentrosymmetric superconductors, Phys. Rev. Lett. **105**, 097002 (2010).

[156] K. Yada, M. Sato, Y. Tanaka, and T. Yokoyama, Surface density of states and topological edge states in noncentrosymmetric superconductors, Phys. Rev. B **83**, 064505 (2011).

[157] M. Sato, Y. Tanaka, K. Yada, and T. Yokoyama, Topology of Andreev bound states with flat dispersion, Phys. Rev. B **83**, 224511 (2011).

[158] T. Kokkeler, A. Hijano, and F. S. Bergeret, Anisotropic differential conductance of a mixed-parity superconductor/ferromagnet structure, Phys. Rev. B **107**, 104506 (2023).

[159] M. A. Gijs and G. E. Bauer, Perpendicular giant magnetoresistance of magnetic multilayers, Adv. Phys. **46**, 285 (1997).

[160] M. Božović and Z. Radović, Coherent effects in double-barrier ferromagnet/superconductor/ferromagnet junctions, Phys. Rev. B **66**, 134524 (2002).

[161] T. Miyazaki and N. Tezuka, Giant magnetic tunneling effect in Fe/Al_2O_3/Fe junction, J. Magn. Magn. Mater. **139**, L231 (1995).

[162] G. Binasch, P. Grünberg, F. Saurenbach, and W. Zinn, Enhanced magnetoresistance in layered magnetic structures with antiferromagnetic interlayer exchange, Phys. Rev. B **39**, 4828 (1989).

[163] M. A. M. Gijs, S. K. J. Lenczowski, and J. B. Giesbers, Perpendicular giant magnetoresistance of microstructured Fe/Cr magnetic multilayers from 4.2 to 300 k, Phys. Rev. Lett. **70**, 3343 (1993).

[164] W. P. Pratt, S.-F. Lee, J. M. Slaughter, R. Loloee, P. A. Schroeder, and J. Bass, Perpendicular giant magnetoresistances of Ag/Co multilayers, Phys. Rev. Lett. **66**, 3060 (1991).

[165] G. E. W. Bauer, Perpendicular transport through magnetic multilayers, Phys. Rev. Lett. **69**, 1676 (1992).

[166] T. Valet and A. Fert, Theory of the perpendicular magnetoresistance in magnetic multilayers, Phys. Rev. B **48**, 7099 (1993).

[167] R. K. Kushwaha, A. S. Sharma, S. Srivastava, P. K. Meena, M. Pula, J. Beare, J. Gautreau, A. D. Hillier, G. M. Luke, and R. P. Singh, Broken time-reversal symmetry in a new non-centrosymmetric superconductor Re8NbTa, arXiv:2401.07614.

[168] K. Chen, Z. Zhu, Y. Xie, A. D. Hillier, J. S. Lord, P. Dai, and L. Shu, Multicondensate lengths with degenerate excitation gaps in $BaNi_2As_2$ revealed by muon spin relaxation study, Phys. Rev. B **109**, 024513 (2024).

[169] K. V. Samokhin, Effects of impurities on the upper critical field H_{c2} in superconductors without inversion symmetry, Phys. Rev. B **78**, 144511 (2008).

[170] K. V. Samokhin, Upper critical field in noncentrosymmetric superconductors, Phys. Rev. B **78**, 224520 (2008).

[171] K. V. Samokhin, NMR relaxation rate in noncentrosymmetric superconductors, Phys. Rev. B **72**, 054514 (2005).

[172] N. Aso, H. Miyano, H. Yoshizawa, N. Kimura, T. Komatsubara, and H. Aoki, Incommensurate magnetic order in the pressure-induced superconductor $CeRhSi_3$, J. Magn. Magn. Mater. **310**, 602 (2007).

[173] N. Hayashi, K. Wakabayashi, P. A. Frigeri, and M. Sigrist, Nuclear magnetic relaxation rate in a noncentrosymmetric superconductor, Phys. Rev. B **73**, 092508 (2006).

[174] A. Pustogow, Y. Luo, A. Chronister, Y.-S. Su, D. A. Sokolov, F. Jerzembeck, A. P. Mackenzie, C. W. Hicks, N. Kikugawa, S. Raghu, E. D. Bauer, and S. E. Brown, Constraints on the superconducting order parameter in Sr_2RuO_4 from oxygen-17 nuclear magnetic resonance, Nature (London) **574**, 72 (2019).

[175] F. S. Bergeret, M. Silaev, P. Virtanen, and T. T. Heikkilä, Colloquium: Nonequilibrium effects in superconductors with a spin-splitting field, Rev. Mod. Phys. **90**, 041001 (2018).

[176] R. Dingle, The electrical conductivity of thin wires, Proc. R. Soc. London A **201**, 545 (1950).

[177] V. Gantmakher, *Electrons and Disorder in Solids*, translated by L. I. Man (Oxford University Press, Oxford, 2005), Vol. 130.

[178] W. Belzig, F. K. Wilhelm, C. Bruder, G. Schön, and A. D. Zaikin, Quasiclassical Green's function approach to mesoscopic superconductivity, Superlattices Microstruct. **25**, 1251 (1999).

[179] V. Chandrasekhar, Proximity-coupled systems: Quasiclassical theory of superconductivity, in *Superconductivity: Conventional and Unconventional Superconductors*, edited by K. H. Bennemann and J. B. Ketterson (Springer, Berlin, 2008), pp. 279–313.

[180] A. Schmid and G. Schön, Linearized kinetic equations and relaxation processes of a superconductor near T_c, J. Low Temp. Phys. **20**, 207 (1975).

[181] T. T. Heikkilä, M. Silaev, P. Virtanen, and F. S. Bergeret, Thermal, electric and spin transport in superconductor/ferromagnetic-insulator structures, Prog. Surf. Sci. **94**, 100540 (2019).

[182] Y. Tanaka, Y. V. Nazarov, and S. Kashiwaya, Circuit theory of unconventional superconductor junctions, Phys. Rev. Lett. **90**, 167003 (2003).

[183] Y. Tanaka, Y. V. Nazarov, A. A. Golubov, and S. Kashiwaya, Theory of charge transport in diffusive normal metal/unconventional singlet superconductor contacts, Phys. Rev. B **69**, 144519 (2004).

[184] Y. V. Nazarov, Novel circuit theory of Andreev reflection, Superlattices Microstruct. **25**, 1221 (1999).

[185] T. H. Kokkeler, Y. Tanaka, and A. A. Golubov, Spin-projected charge conductance in SNN junctions with noncentrosymmetric superconductors, Phys. Rev. Res. **5**, L012022 (2023).

[186] Y. Tanaka, S. Tamura, and J. Cayao, Theory of majorana zero modes in unconventional superconductors, arXiv:2402.00643.

[187] F. S. Bergeret, A. F. Volkov, and K. B. Efetov, Long-range proximity effects in superconductor-ferromagnet structures, Phys. Rev. Lett. **86**, 4096 (2001).

[188] M. Kuprianov and V. Lukichev, Influence of boundary transparency on the critical current of dirty SS'S structures, Zh. Eksp. Teor. Fiz **94**, 149 (1988).

[189] F. S. Bergeret, A. F. Volkov, and K. B. Efetov, Enhancement of the Josephson current by an exchange field in superconductor-ferromagnet structures, Phys. Rev. Lett. **86**, 3140 (2001).

[190] M. Sato and Y. Ando, Topological superconductors: A review, Rep. Prog. Phys. **80**, 076501 (2017).

[191] M. Leijnse and K. Flensberg, Introduction to topological superconductivity and Majorana fermions, Semicond. Sci. Technol. **27**, 124003 (2012).

[192] Y. Tanaka, T. Yokoyama, A. V. Balatsky, and N. Nagaosa, Theory of topological spin current in noncentrosymmetric superconductors, Phys. Rev. B **79**, 060505(R) (2009).

[193] The theory used to describe the SFN junctions is based on quasiclassical theory, and therefore assumes that the Fermi energy is well within a band and the density of states is not a rapidly varying function near the Fermi surface, and the Fermi energy is the largest energy scale in the problem.

[194] C.-T. Wu and K. Halterman, Spin transport in half-metallic ferromagnet-superconductor junctions, Phys. Rev. B **98**, 054518 (2018).

[195] R. Dawson and V. Aji, Proximity effect of *s*-wave superconductor on inversion broken Weyl semi-metal, arXiv:2312.00187.

[196] J.-S. Zhou, L. G. Marshall, Z.-Y. Li, X. Li, and J. M. He, Weak ferromagnetism in perovskite oxides, Phys. Rev. B **102**, 104420 (2020).